ALMA MATER STUDIORUM – UNIVERSITA' DI BOLOGNA

DIPARTIMENTO DI INGEGNERIA DELL'ENERGIA ELETTRICA E DELL'INFORMAZIONE
"GUGLIELMO MARCONI"

DOTTORATO DI RICERCA IN INGEGNERIA BIOMEDICA, ELETTRICA E DEI SISTEMI
XXX CICLO

Settore Concorsuale: 09/E1
Settore Scientifico Disciplinare: ING-IND/31

ELECTROHYDRODYNAMIC-DRIVEN MASS TRANSPORT ENHANCEMENT IN ATMOSPHERIC-PRESSURE AIR SURFACE DIELECTRIC BARRIER DISCHARGES

Candidato:
Matteo Taglioli

Coordinatore:
Prof. Daniele Vigo

Relatore:
Prof. Carlo Angelo Borghi

Esame finale anno 2018

Acknowledgements

Firstly, I would like to express my sincere gratitude to my advisor Prof Carlo Angelo Borghi for the continuous support, motivation and immense knowledge.

Besides my advisor, I would like to thank Dr Gabriele Neretti for his insightful comments and hard questions that allowed me to widen my research from various perspectives.

My sincere thanks also goes to Dr Felipe Iza, who provided me the opportunity to join his research team as intern and gave me access to his facilities. It would not have been possible to conduct this study without his precious contribution.

I thank British colleagues of mine Alexander Shaw, Alexander Wright and Junchen Ren for the stimulating discussions and all the fun we had together when I joined them in Loughborough.

Lastly, I would like to thank my family for supporting me spiritually throughout these intense years of research and my life in general.

Matteo Taglioli, PhD Researcher

Department of Electrical, Electronic and Information Engineering

University of Bologna

Contents

Abstract

Low-temperature plasmas technology can be useful in quite different areas of daily life and industrial production. Cold atmospheric-pressure plasmas have recently become subject of great interest for a wide variety of applications, including surface treatment and thin-film deposition. A driving force for development of room-temperature plasma applications is the avoidance of expensive equipment required for competing vacuum-based plasma technologies.

During the last two decades, atmospheric-pressure electric gas discharges have drawn a lot of attention for their potential applications. In particular, surface dielectric barrier discharge plasmas have received renewed interest in recent years for emerging biomedical, environmental and agricultural applications.

In most of these processes, plasma is not in direct contact with the target being treated and reactive species transport to the substrate is typically assumed to be diffusion-controlled. This study shows how to engineer electrode patterns in order to take advantage of electrohydrodynamic forces and enhance reactive species delivery towards target under treatment.

Novel surface dielectric barrier discharge devices with annular electrodes of diameter varying from 10mm to 50mm were fabricated. All devices were operated in atmospheric-pressure air, thereby leading to several reactive oxygen and nitrogen oxidising chemical compounds formation.

Plasma local properties and electrohydrodynamic forces were experimentally investigated by means of electrical, optical and fluid-dynamics diagnostics. Reactive species delivery provided by devices was studied using several different chemical

essays. Although all devices were driven at constant power density, therefore presenting constant plasma local properties, a 3-fold efficacy enhancement was observed for 30mm electrode diameter device.

Biocidal efficacy of annular surface dielectric barrier discharge plasmas was tested as well by treating *Candida albicans*, which in turn is one of the most widespread and severe causes of skin and superficial mucosal infections. A 5-log reduction in the bacterial load was achieved after 5min of exposure to 30mm electrode diameter device powered with ~4W.

Results presented and discussed in this work are quite encouraging. As it still remains an open challenge to generate uniform cold atmospheric-pressure plasma discharges, this study might provide basis for further research efforts addressing process scale-up and development of plasma devices for in-field large area biocidal purposes.

Figures and tables

Chapter 1
Introduction

Conventional sterilisation methods, including wet and dry heat, irradiation or chemical gases, have several drawbacks [1]. Firstly, several substrate properties, such as molecular weight, volume, and morphology, can be negatively altered by these sterilisation processes. This can therefore influence physical and biological performance of sterlised items, leading to failure. In addition, conventional sterilisation methods require a 120°C or higher operating temperature, which causes degradation of heat-sensitive substrates. Lastly, another crucial limitations are the need for expensive vacuum equipment and the use of toxic gases, like formaldehyde or ethylene oxide

Cold atmospheric-pressure plasma technology does not present these disadvantages [2]. Plasmas operated at atmospheric pressure are characterised by temperature below 40°C and do not lead to harmful chemical byproducts. Cold atmospheric-pressure plasmas properties permit therefore eco-friendly sterilisation process of thermolabile substrates [3] and allow in vivo treatments, opening a new and larger spectrum of possible applications. The first devices developed have already proven their biocidal properties [4-10] both in vitro, ex vivo, and in vivo.

Plasma is known as the fourth state of matter and it is basically an electrically-neutral ionised gas. One of the most attractive features of cold atmospheric-pressure plasmas is their capability to enhance chemical processes without the need for high temperatures. In addition, their design simplicity and low operational costs provide the basis for a large variety of biological applications.

Cold atmospheric-pressure plasmas have been established to be energy-efficient and eco-friendly novel tools for the simultaneous production of intense UV radiation and several reactive oxygen and nitrogen oxidising species [11,12] including ozone, hydroxyl radical and hydrogen peroxide. All these active agents (figure 1) are effective against pathogens, thereby making low-temperature plasmas a powerful technology to treat contaminated matter [13,14].

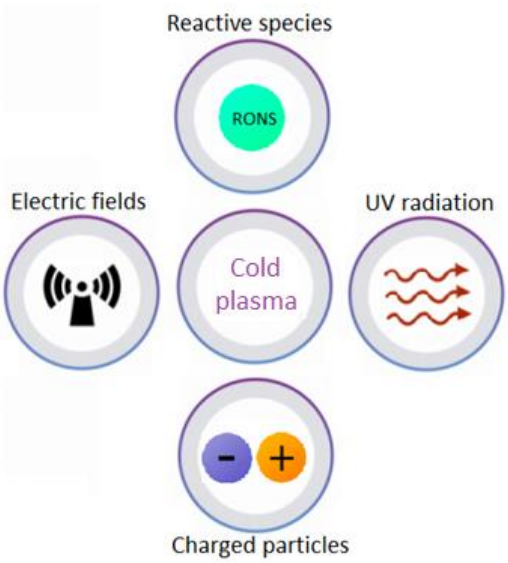

Figure 1. Biocidal agents produced in cold atmospheric-pressure plasmas.

Different active agents are more or less important according to the type of treatment. When plasma is directly applied to the biological substrate, charged particles and local electric field may have important effects. Conversely, in indirect treatments only chemically reactive species and UV radiation participate in the sterilisation process.

Cold atmospheric-pressure plasma sterilisation is a complicated process because it involves a wide variety of mechanisms. Initial steps in understanding possible interaction pathways have been made over the last decade [15,16], but many parts of the process still remain unclear. Cellular membrane (figure 2) is the outermost barrier separating pathogens cell interior from its environment, therefore it represents the most important biological object in the interaction between cold

atmospheric-pressure plasmas and microorganisms. Various processes may occur at cell membrane during the exposure to a room-temperature plasma. Electric fields and charged particles penetrating cell membrane may cause electroporation. Membrane damage is induced by the oxidising action of chemically reactive species as well.

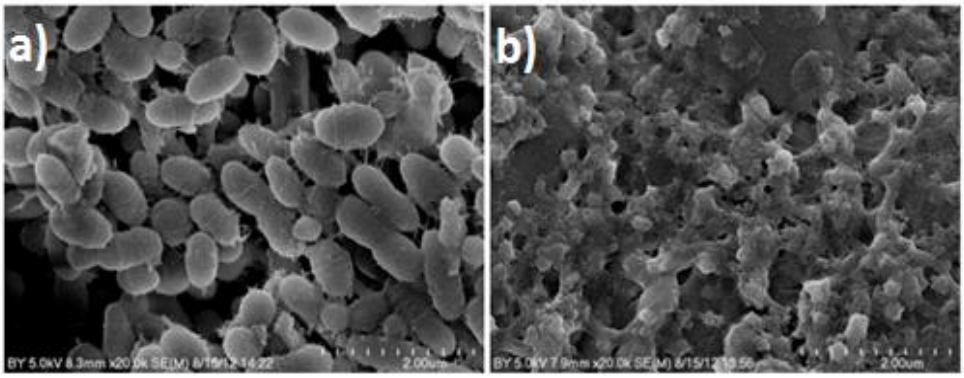

Figure 2. *Staphylococcus aureus* membrane before a) and after b) exposure to a cold atmospheric-pressure plasma discharge.

Pathogens are rarely in dry environment, therefore interaction between cold atmospheric-pressure plasmas and liquids must be considered as well. Indeed, sterilising effects on pathogens may also occur due to chemical modification of the surrounding medium [17,18].

Biocidal efficacy of low-temperature plasmas interacting with liquids may be explained by a dual mechanism (figure 3). On the one hand, pathogens cell membrane damage is still induced by the same processes occurring in dry environment and several powerful chemically active compounds are formed directly in the liquid as well. On the other hand, nitrogen reactive species promotes acidification, thereby enhancing oxidising potential of liquid surrounding pathogens. Chemical composition of liquid as well as concentration and nature of reactive species generated in the plasma discharge play major role in the process.

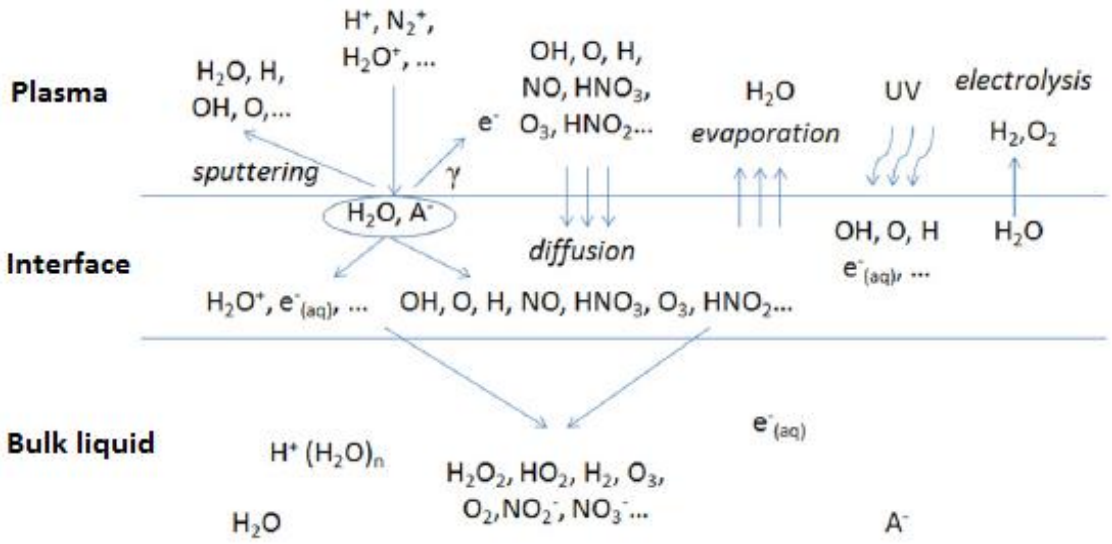

Figure 3. Chemical processes involved in the interaction between cold atmospheric-pressure plasmas and water.

There are many different methods to generate plasmas in laboratory, but the most common process is electric gas discharge ignition. When delivering electrical power into a neutral gas like air, a fraction of gas atoms become ionised and an electric gas discharge is fired. The simplest and most efficient way to ignite an electric gas discharge is to supply a couple of spaced electrodes with a voltage source. Electric field accelerates free electrons to energies sufficiently high to ionise other atoms by collision, thereby leading to gas breakdown.

Although electric gas breakdown mechanism is very sophisticated, it usually starts with an electron avalanche (figure 4), i.e. multiplication of some primary electrons in cascade ionisation. Electron avalanches produce an electric current flow through the gas, thereby making it an electrically-conductive medium.

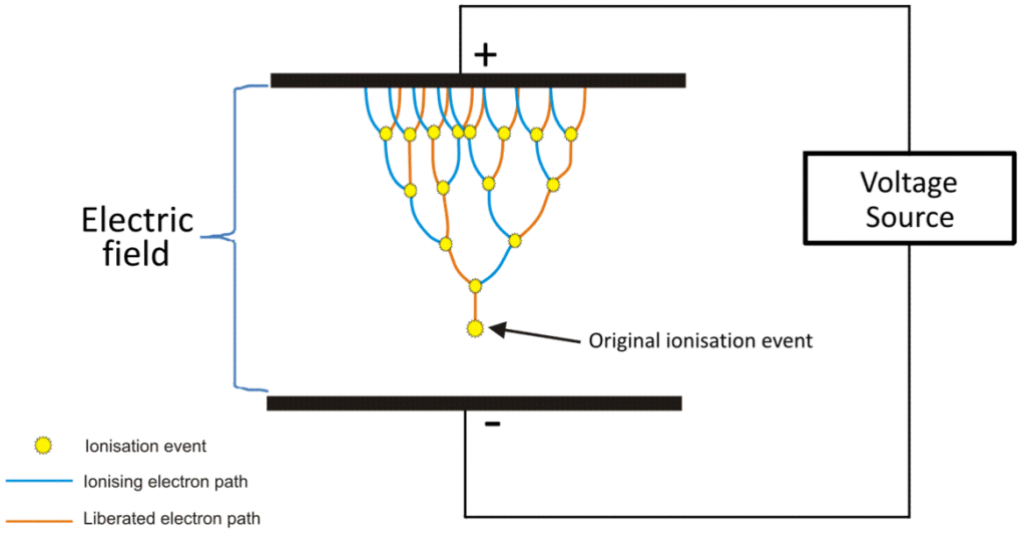

Figure 4. Cascade impact ionisation between two electrodes supplied by a voltage source.

Electric gas breakdown occurs only when the applied electric field exceeds gas dielectric strength. Dielectric strength of a gas strongly depends on its pressure (figure 5). Mean free path between collisions is larger at low pressure, therefore electrons gain more energy from electric field and ionisation process is more efficient. In addition, molecular gases like air usually present higher dielectric strength than monoatomic gases at given pressure.

Even though ignition of a low-pressure electric gas discharge needs lower voltages, atmospheric-pressure operation is preferred in applications in order to avoid employment of expensive and complex vacuum systems. Moreover, atmospheric-pressure electric gas discharges usually present strong thermodynamic non-equilibrium. Electrons are highly energetic, but plasma gas is nearly room temperature without any additional cooling.

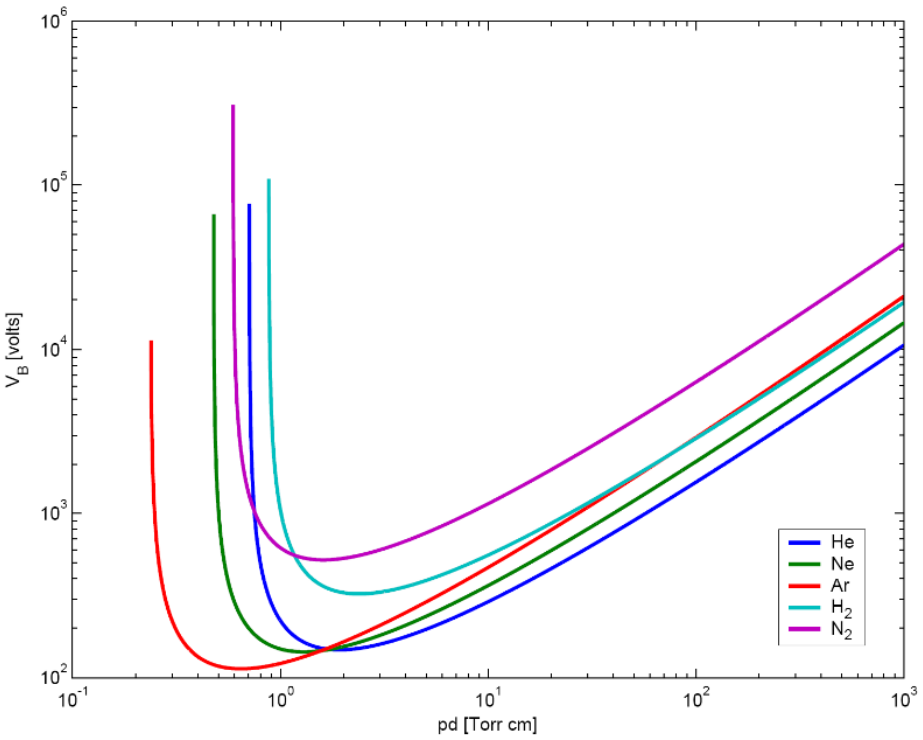

Figure 5. Paschen's curve for several gases.

Gas type	Degrees of freedom
Monoatomic	3 translational 0 rotational 0 vibrational
Diatomic	3 translational 2 rotational 1 vibrational

Table 1. Monoatomic and diatomic gases degrees of freedom.

Temperature is one of the key parameters characterising electric gas discharges and determines the application. Temperature in plasmas is defined by average energies of particles and their degrees of freedom (table 1). As multi-component systems, electric gas discharges are therefore able to exhibit multiple temperatures. Although relation between different temperatures in atmospheric-pressure plasma discharges can be complex, it is conventionally presented as follows. Electron

temperature is the highest in the system, followed by temperature of vibrational excitation of molecules. The lowest temperature is usually shared by heavy neutrals, ions and rotational degrees of freedom. In atmospheric-pressure electric gas discharges electron temperature is ~1eV, whereas gas temperature must be kept close to room temperature.

However, gas breakdown process at atmospheric pressure may result in formation of arcs and sparks (figure 6), especially in molecular gases like air. Arcing and sparking lead to strongly unstable hot discharges. Arcs and sparks are therefore not desirable in applications, since high temperatures may damage both plasma device and substrate being treated. There are several options to avoid arcing and sparking, but the most useful approach is represented by dielectric barrier discharge arrangement.

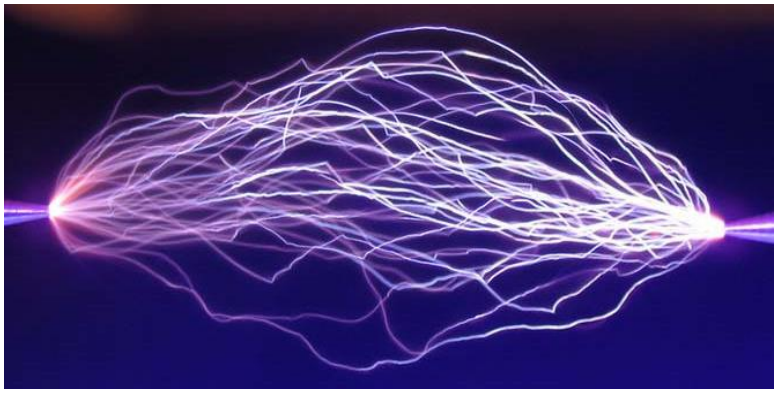

Figure 6. Arcs and sparks in an atmospheric-pressure air plasma discharge between two pointed electrodes.

Dielectric barrier discharges have been studied for more than a century. First experimental results were reported by Siemens in 1857 [19]. He discovered that atmospheric-pressure air dielectric barrier discharges are powerful tools for ozone generation. Ozone production was the major application of atmospheric-pressure air dielectric barrier discharge plasmas until about ten years ago. Extensive research activities carried out in the last few years resulted both in improved ozone generators and in a number of biological applications [20,21].

Strong thermodynamic non-equilibrium with low gas temperatures and simple scalability are distinctive features of atmospheric-pressure dielectric barrier discharges. Air gap between electrodes is usually a few millimetres wide to ensure stable plasma formation (figure 7).

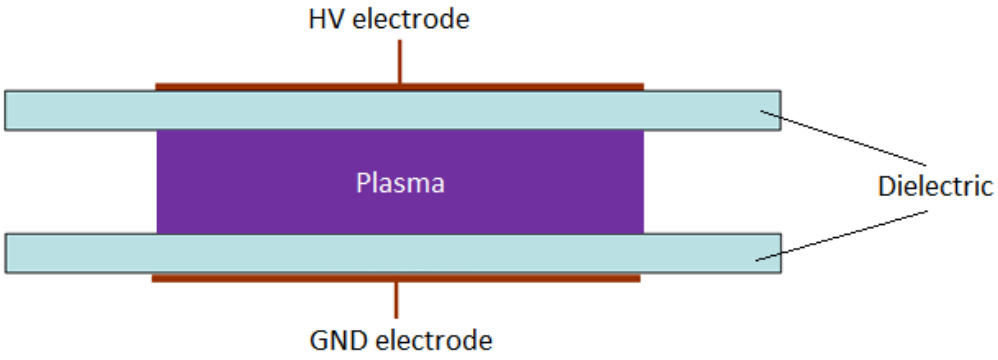

Figure 7. Dielectric barrier discharge arrangement with two insulating layers.

Dielectric barrier discharge devices always include at least one insulating layer. Atmospheric-pressure air operation of dielectric barrier discharges (figure 8) result in several micro-discharges randomly developing in the gap between electrodes due to charge seeding on dielectric (table 2).

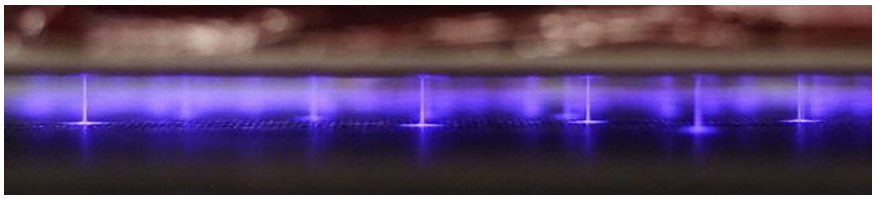

Figure 8. Micro-discharges in atmospheric-pressure air dielectric barrier discharge plasmas.

The presence of insulating layers requires AC or pulsed excitation of dielectric barrier discharge devices. Atmospheric-pressure air dielectric barrier discharge plasmas are usually powered by sinusoidal voltages in kV range at kHz frequency both in continuous and discontinuous mode.

Dielectric layers produce a displacement current that is overlapped by multiple current pulses due to micro-discharges formation (figure 9). Plasma ignites as soon as

breakdown voltage is reached in the discharge gap and last until applied voltage module increases.

Duration	1-10ns
Radius	~100µm
Peak current	~100mA
Electric charge	0.1-1nC
Electron density	10^{14}-10^{15}cm^{-3}
Electron energy	1-10eV
Gas temperature	300-400K

Table 2. Atmospheric-pressure air dielectric barrier discharge plasmas properties.

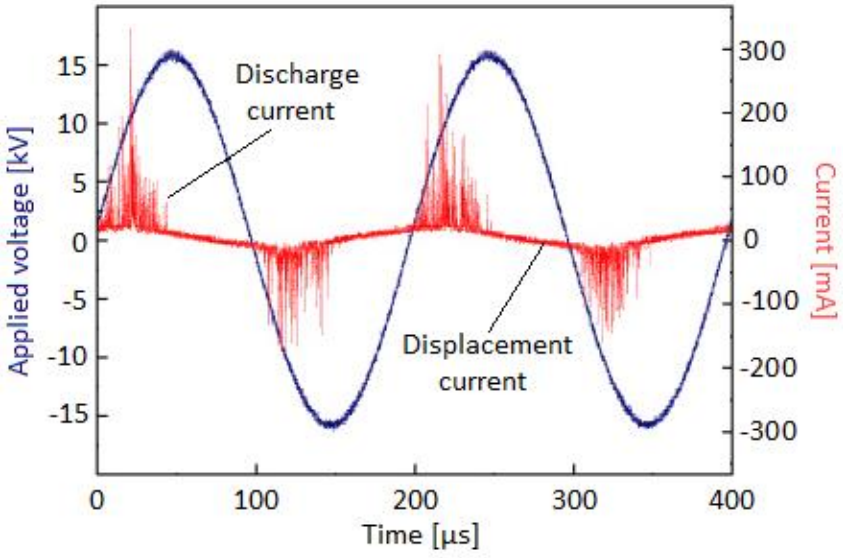

Figure 9. Time-resolved applied voltage and current signals of a sinusoidal atmospheric-pressure air dielectric barrier discharge plasma.

Electric charge build-up onto insulating layers due to plasma formation decreases air gap voltage, thereby quenching the discharge and preventing arcs and sparks formation. Applied voltage polarity must be inverted to push seeded electrons again into air gap and fire another discharge in the subsequent half-cycle.

As mentioned above, many investigations on atmospheric-pressure air dielectric barrier discharges were aimed at improving ozone generation in the first place. Plasma local properties must be optimized in order to enhance ozone production. The major fraction of electrons energy is firstly deposited in atomic and molecular states excitation of O_2 and N_2. Ozone is then formed in the following three-body reaction

$$O + O_2 + M \rightarrow O_3 + M$$

where *M* is a third collision partner. However, ozone generation in atmospheric-pressure air dielectric barrier discharge plasmas is limited by undesired side reactions taking place, which consume oxygen atoms or deplete O_3 molecules. The presence of N_2 and its atomic and molecular excited species add to the complexity of chemical kinetics, thereby resulting in formation of a large variety of nitrogen oxides, including NO, N_2O, NO_2, NO_3 and N_2O_5. Excitation and dissociation of N_2 molecules lead to a number of additional reaction paths involving nitrogen and its excited molecular states that produce oxygen atoms available for ozone generation. About half of O_3 formed in atmospheric-pressure air dielectric barrier discharges results from these indirect processes.

Ozone formation in atmospheric-pressure air dielectric barrier discharge plasmas breaks down completely above a certain concentration of nitrogen oxides. This phenomenon is referred to as discharge poisoning. Discharge poisoning condition is characterised by rapid nitrogen oxides reactions, consuming oxygen atoms at a faster rate than ozone formation mechanism. The result is an accelerated recombination of O atoms, catalysed by the presence of nitrogen oxides. Previously formed ozone is removed in a catalytic destruction process involving NO and NO_2. Nitrogen oxides reactions are extremely fast so that relatively small concentrations may seriously interfere with ozone formation. High temperature in discharge gap due

to excessive power absorbed by plasma enhances nitrogen oxides synthesis in atmospheric-pressure air dielectric barrier discharges, thereby leading to reduced ozone generation.

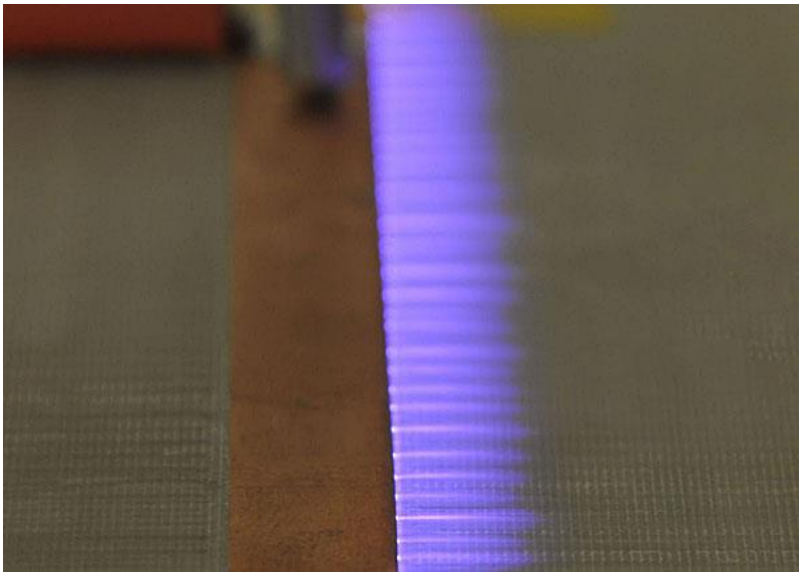

Figure 10. Atmospheric-pressure air surface dielectric barrier discharge plasma.

Closely related to dielectric barrier discharges are surface dielectric barrier discharge plasmas, which are generated along insulating surfaces imbedded by two electrodes (figure 10). Atmospheric-pressure air surface dielectric barrier discharges have been widely investigated in the past two decades for airflow manipulation [22] due to their mechanical simplicity, electrical control capability and low power consumption.

In atmospheric-pressure air surface dielectric barrier discharge devices for airflow control, momentum transfer from charged to neutral particles results in an electrohydrodynamic body force, a phenomenon also known as electric wind (figure 11). Electric wind typically imparts momentum to background air tangentially to dielectric surface. Electrical and geometrical variations can also produce fluxes in other directions [23,24], though.

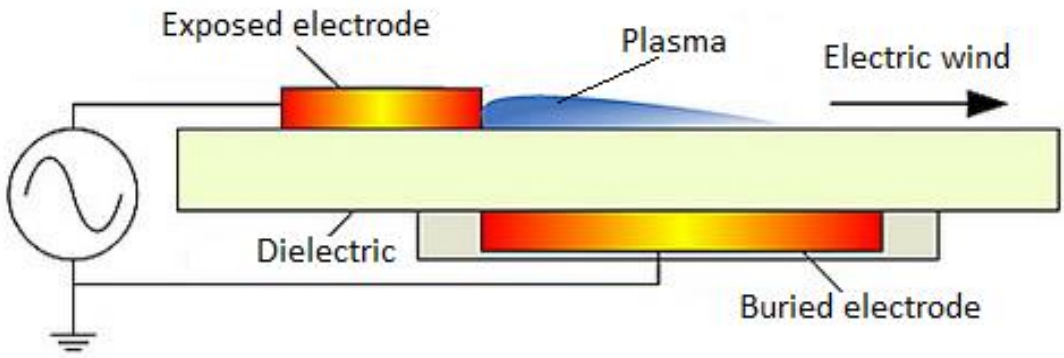

Figure 11. Electric wind in an atmospheric-pressure surface dielectric barrier discharge device for airflow control.

In addition to flow control, atmospheric-pressure air surface dielectric barrier discharge plasmas have gained renewed interest in recent years for their potential use in emerging biological applications [25-29]. In most of these applications, plasma is not in direct contact with substrate being treated and reactive species delivery is usually assumed to be diffusion-controlled [30,31].

This work demonstrates that generally this is not the case and that atmospheric-pressure air surface dielectric barrier discharges can be designed to enhance reactive species transport onto target under treatment by taking advantage of electrohydrodynamic forces. An in-depth characterisation of plasma device is carried out in order to optimize reactive species delivery towards substrate being treated and its biocidal efficacy is tested as well.

Chapter 2
Annular surface dielectric barrier discharge plasmas

Although all surface dielectric barrier discharges have the same underlying topology, a number of different electrode designs have been proposed in recent years for biological applications [32,33]. To date, however, limited attention has been paid to electrode geometry influence on the efficacy of these devices.

Tangential fluxes colliding with each other in linear or annular electrode arrangement can generate a so-called synthetic jet perpendicular to dielectric layer (figure 12). This feature can be employed to direct plasma reactive species towards substrates under treatment.

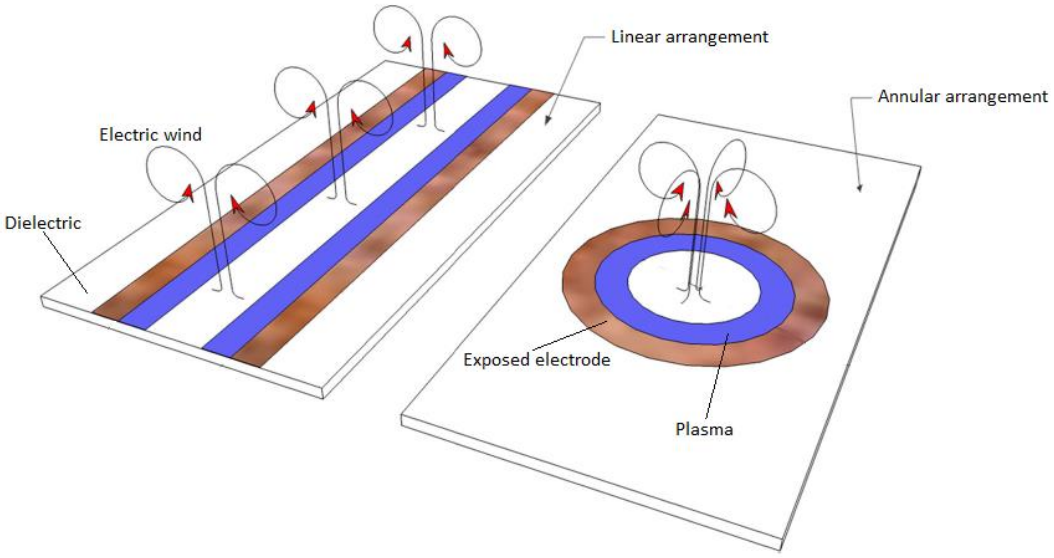

Figure 12. Linear and annular arrangements of surface dielectric barrier discharge devices.

Annular designs have already been demonstrated to induce stronger electrohydrodynamic forces than linear arrangement [34,35]. This work is therefore focused on development and characterisation of annular surface dielectric barrier discharges for biological applications.

Plasma devices studied in this work were fabricated using a 1.5mm thick glass-reinforced epoxy FR-4 substrate as dielectric barrier, with circular and annular copper electrodes laminated on either sides (figure 13). Ground electrode and outer part of high-voltage one were buried in epoxy resin to avoid plasma formation in those areas and, as a result, discharge ignites only inside annular region (figure 14).

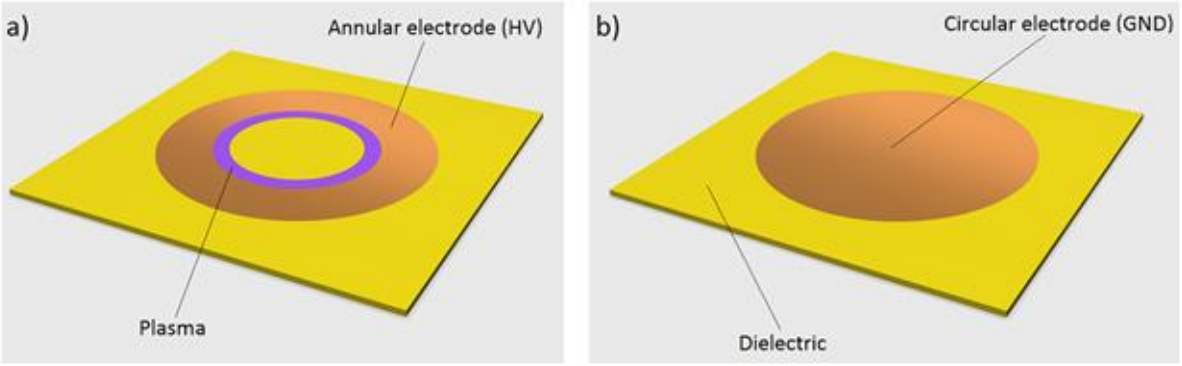

Figure 13. Side a) and side b) 3D rendering of an annular surface dielectric barrier discharge.

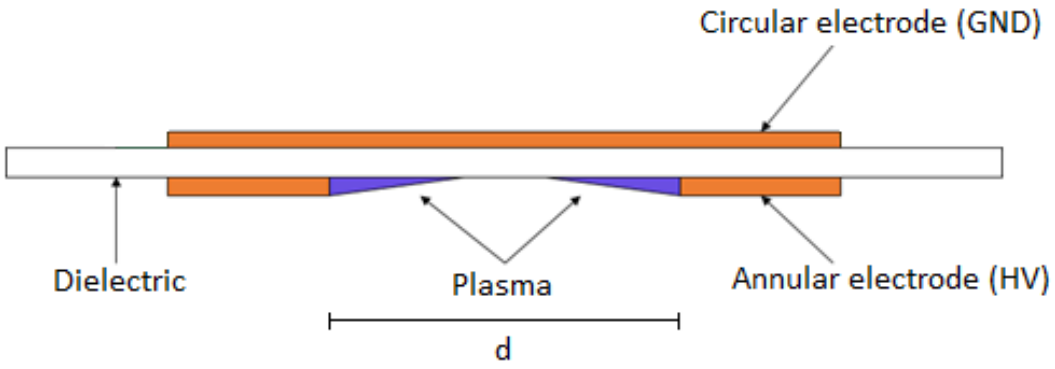

Figure 14. Cross section schematic of an annular surface dielectric barrier discharge.

Plasma was powered in atmospheric-pressure air, thereby leading to formation of a reactive oxygen and nitrogen reactive species admixture. Several devices with different electrode diameter were fabricated to investigate plasma local properties and study influence of electrode geometry on reactive species delivery onto target under treatment.

Plasma was excited by a 11.5kV$_p$ sinusoidal voltage at 5kHz (figure 15) both in continuous and discontinuous modes. Discontinuous mode operation was obtained by modulating applied voltage with a 500mHz square signal and varying duty cycle.

Duty cycle is defined as ratio between time in which plasma device is active T_{ON} and modulating signal period T_m (figure 16). Duty cycle D can therefore be expressed as

$$D = T_{ON} f_m$$

where $f_m = 1/T_m$ is modulation frequency. Duty cycle is usually given in percent, 100% representing continuous mode operation.

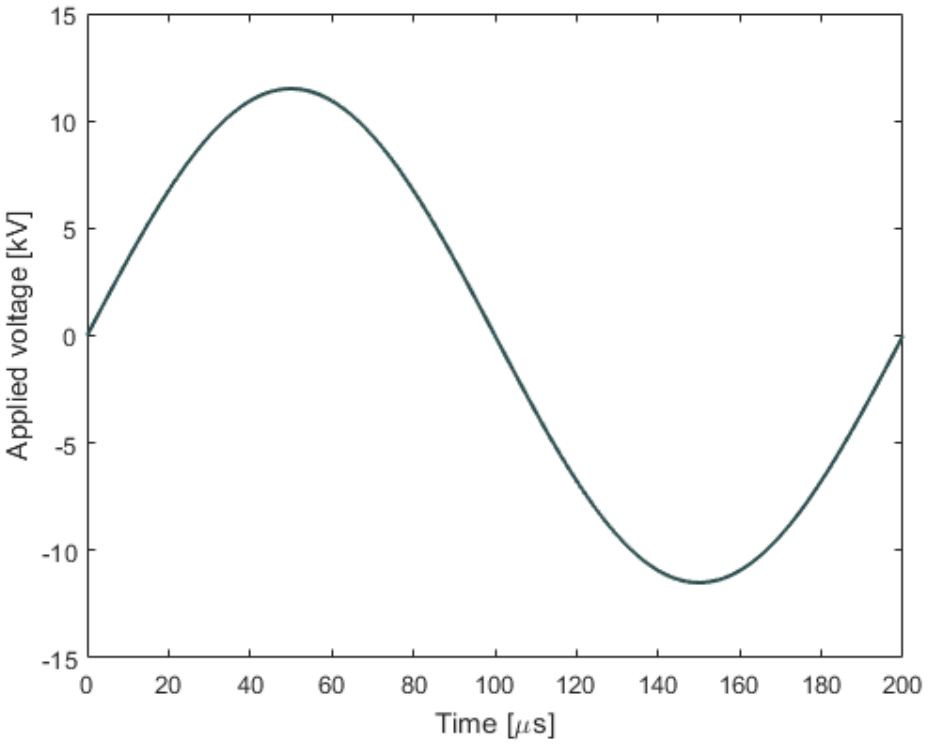

Figure 15. Time-resolved voltage signal powering plasma.

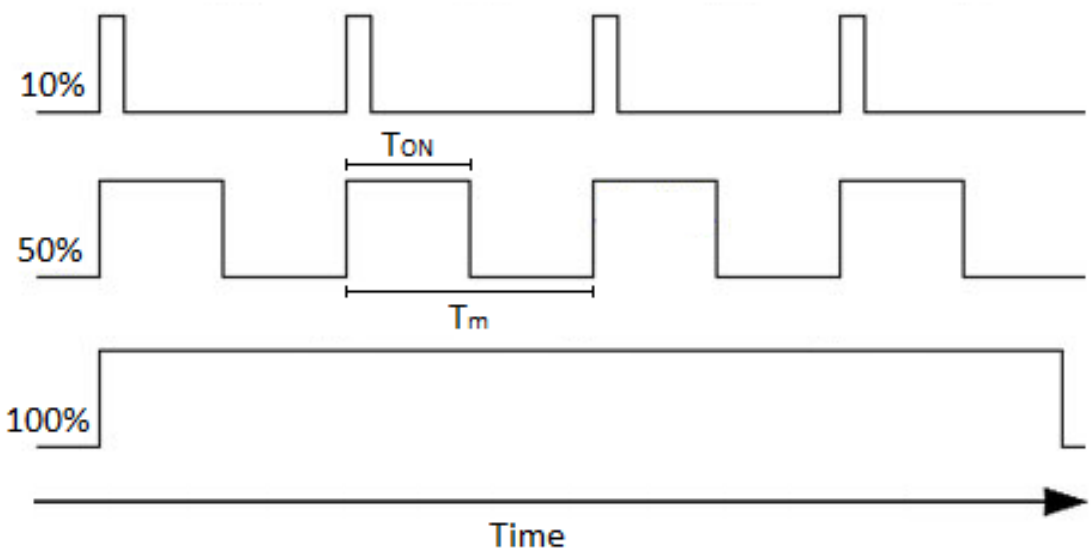

Figure 16. Continuous and discontinuous mode operation of the devices.

Images taken using a CCD camera at fixed exposure time and distance show that plasma extend radially ~3mm in all devices (figure 17).

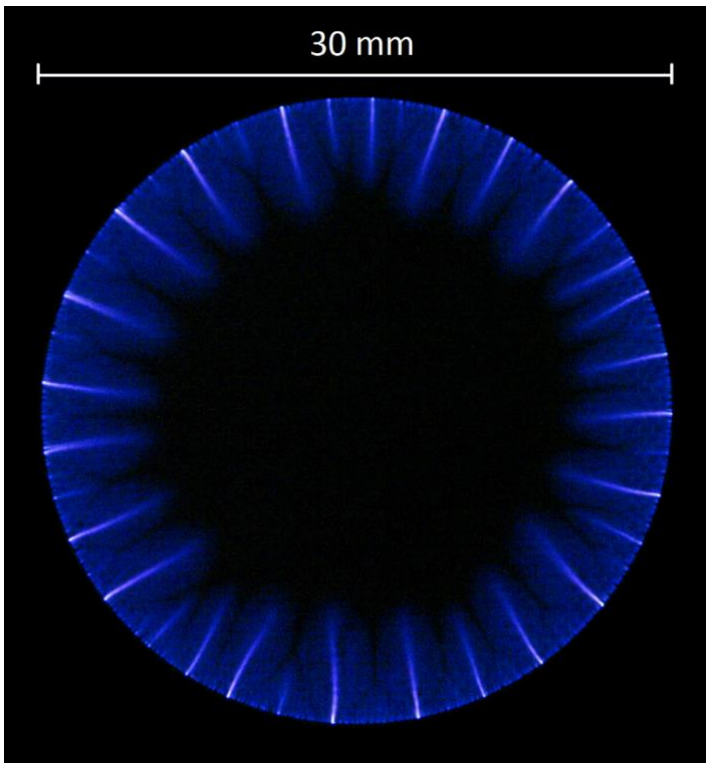

Figure 17. Plasma discharge generated by the 30mm electrode diameter device.

This observation agrees with existing literature where is reported that surface dielectric barrier discharge plasmas radial extension is primarily controlled by applied voltage amplitude [36], which was kept constant in all experiments.

Plasma local properties were studied as a function of electrode diameter and duty cycle. In particular, average power absorbed by discharge and plasma temperature were experimentally investigated.

Time-averaged power delivered to plasmas was evaluated using Lissajous method [37], which involves measuring charge accumulated onto plates of a sensing capacitor connected in series with plasma device. Average power *P* dissipated in plasma is by definition

$$P = \frac{D}{T}\int_0^T v(t)i(t)dt$$

where *D* is the duty cycle, *T* is applied voltage *v(t)* period and *i(t)* is discharge current. If the sensing capacitance value *C* is sufficiently larger than that of plasma device and considering that *v(t)* is sinusoidal, discharge current can be expressed as

$$i(t) = C\frac{dv_C(t)}{dt}$$

where $v_C(t)$ is voltage across sensing capacitor. Average power delivered to plasma can therefore be evaluated as

$$P = \frac{DC}{T}\int_0^T v(t)dv_C(t)$$

, thereby leading to the well-known charge-voltage Lissajous figures.

A 220nF sensing capacitor was connected in series with plasma devices and voltage across it was measured using a Tektronix P6139A voltage probe (figure 18). All devices studied in this work present a capacitance of ~20pF, therefore approximately four orders of magnitude smaller than that of sensing capacitor chosen.

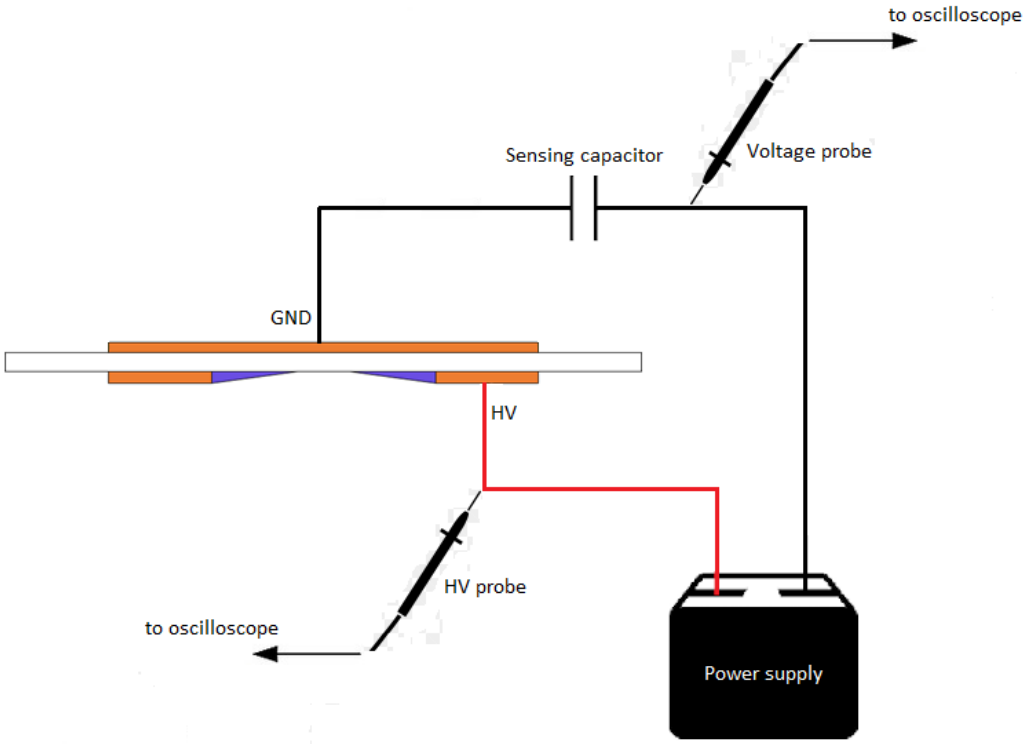

Figure 18. Experimental setup for power measurements.

Applied voltage was measured using a Tektronix P6015A high-voltage probe and both traces were recorded on a Tektronix DPO4104B digital oscilloscope connected to a personal computer. Voltage signals were compensated for different delays introduced by probes before evaluating average power. Measurements were performed in triplicate and experimental error was estimated to be <5%.

Average power delivered to plasma increases linearly with electrode diameter both in continuous and discontinuous mode operation of devices (figure 19). This linear relationship indicates that annular surface dielectric barrier discharges are sustained at constant linear power density.

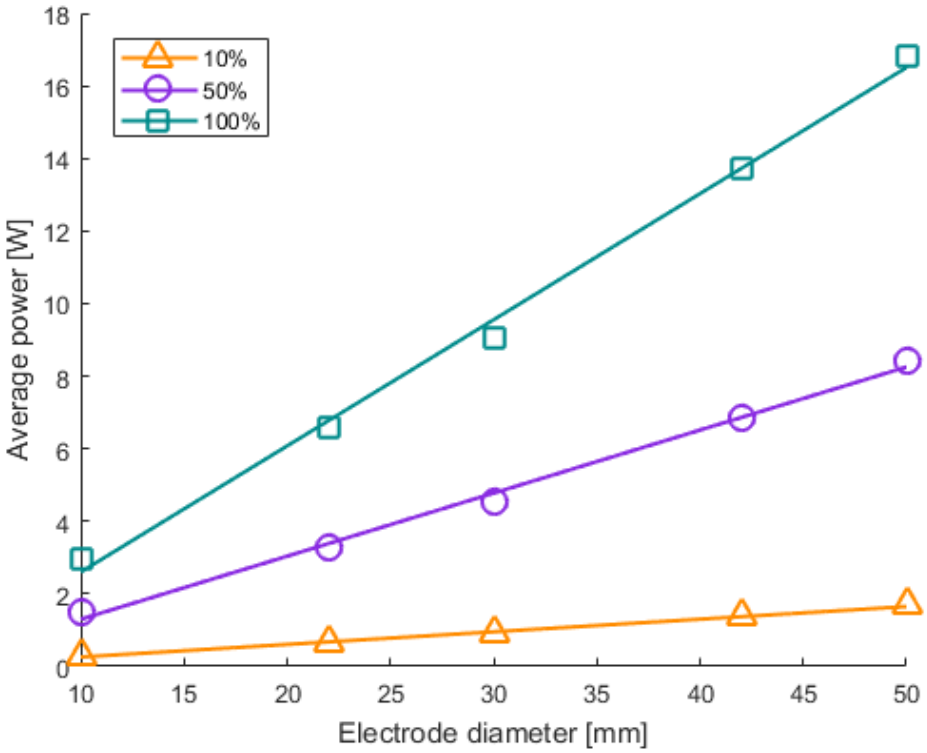

Figure 19. Average power absorbed by plasma as a function of electrode diameter for devices operated at different duty cycle.

Linear power density *p* is a measure of power dissipated per unit plasma length and therefore it can be expressed as

$$p = \frac{P}{\pi d}$$

, i.e. ratio between average power *P* absorbed by discharge and length πd of annular region where plasma forms.

Plasma temperature can be easily evaluated by means of optical emission spectroscopy diagnostic. By non-intrusively detecting light from atomic and molecular transitions occurring in plasma discharges it is possible to identify different chemical species and determine their temperature. Plasma temperature in atmospheric-pressure air electric discharges can be reliably inferred by investigating nitrogen second positive system ro-vibrational transitions [38,39].

Plasma emission spectra of several N_2 second positive system ro-vibrational bands were collected by means of a collimating lens focused on plasma region, a UV/VIS optical fibre connected to a Jobin-Yvon HR460 Czerny-Turner spectrograph (figure 20). Entrance slit and holographic grating were set at 10µm and 2400 lines/mm, respectively. A Stanford Computer Optics 4Picos intensified CCD camera paired to the spectrograph and connected to a personal computer was used as detector. Camera exposure time was set at 100µs and 100 acquisitions were performed for each device. Collected spectra were calibrated both in wavelength and intensity by means of an Ocean Optics HG-1 mercury-argon lamp and an Ocean Optics DH-200-BAL deuterium-halogen light source, respectively.

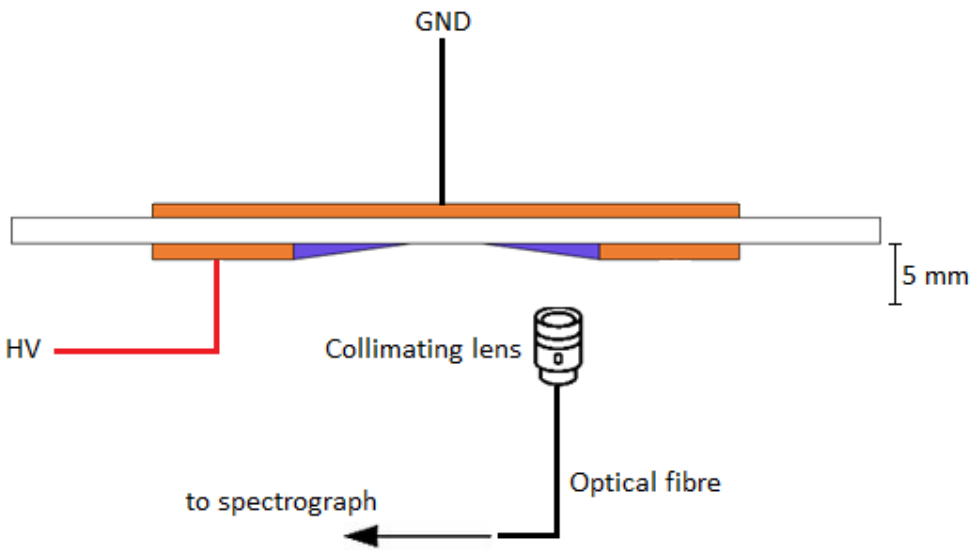

Figure 20. Experimental setup for optical emission spectroscopy.

Plasma temperature is expected to be the same in devices operated at constant linear power density. Indeed optical emission spectra of discharges generated in devices with different electrode diameter sustained at same duty cycle and modulation frequency overlap with each other (figure 21), indicating that plasmas are characterised by same temperature.

A rotational temperature of 360 ± 10 K was evaluated for devices operated at 50% duty cycle by comparing experimental spectra with synthetic ones simulated by means of the software SPECAIR [40].

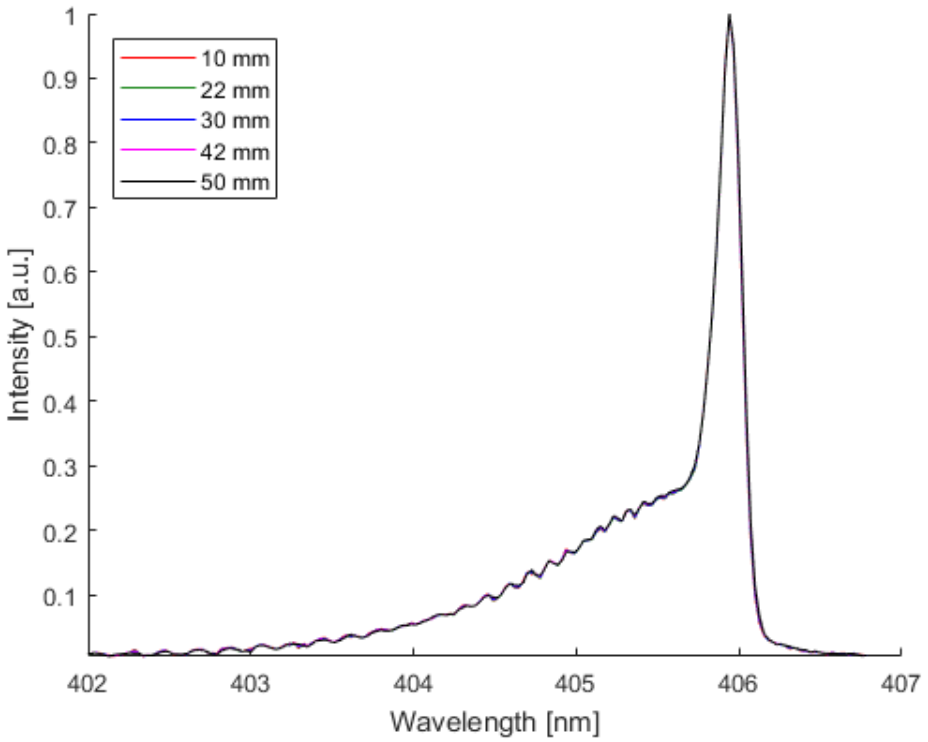

Figure 21. N_2 second positive system (0-3) ro-vibrational transition normalised spectra for discharges generated in devices with different electrode diameter operated at 50% duty cycle.

To conclude, annular surface dielectric barrier discharges with different electrode diameter sustained at same duty cycle and modulation frequency present constant linear power density and plasma temperature.

As evidenced by Arrhenius theory, temperature usually plays the major role in chemical kinetics. Therefore, annular surface dielectric barrier discharge plasmas generated in devices with different electrode diameter and operated in the same conditions are supposed to result in same chemistry.

Chapter 3
Electrohydrodynamic forces in annular surface dielectric barrier discharges

Electrohydrodynamic forces in fabricated annular surface dielectric barrier discharge devices were investigated by means of Pitot tube diagnostic and Schlieren imaging. All results presented in the followings were obtained powering devices in continuous mode with a 11.5kV$_p$ sinusoidal voltage at 5kHz to ensure constant plasma local properties, as already demonstrated in Chapter 1.

Pitot tube diagnostic was used to measure synthetic jets velocity field. Pitot tube is widely employed to determine aircrafts speed and measure gas flow velocity in several industrial applications. It measures local speed at a given point in stream and not average fluid velocity in pipe or conduit.

Pitot tube diagnostic setup consists basically of a tube pointing directly into a fluid flow (figure 22). The moving fluid stagnates inside Pitot tube, as there is no outlet for the flow. As Pitot tube contains fluid, total pressure can be measured. Measuring total pressure only is not useful to determine fluid speed, though. Static pressure must be measured as well to find fluid velocity by means of Bernoulli's equation.

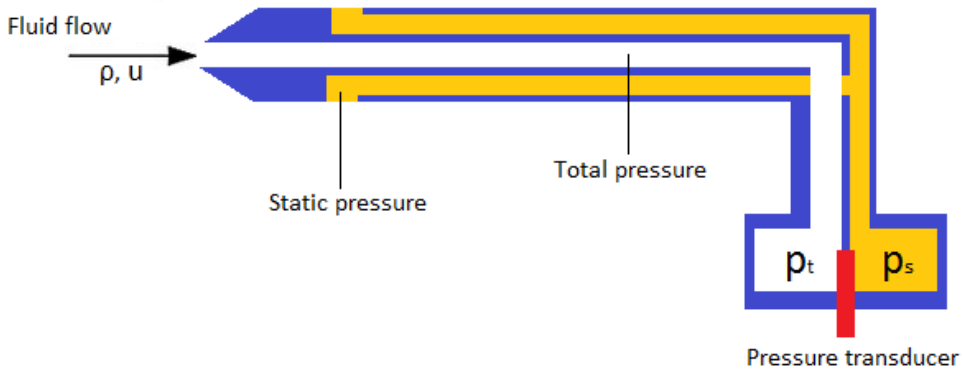

Figure 22. Pitot tube working principle.

Bernoulli's equation states that

$$p_t = p_s + \frac{1}{2}\rho u^2$$

where p_t and p_s are total and static pressure respectively, ρ is fluid density and u is flow velocity. Solving Bernoulli's equation for flow velocity u leads to

$$u = \sqrt{\frac{2(p_t - p_s)}{\rho}}$$

Bernoulli's equation is only valid for fluids that can be treated as incompressible. Liquids are always considered incompressible, whereas gases can be treated as incompressible only under ideal gas behaviour assumption. Deviation from ideal gas behaviour tends to become particularly significant near critical point or in case of very high pressure and very low temperature. Annular surface dielectric barrier discharge devices studied in this work are operated in atmospheric-pressure air and therefore ideal gas behaviour can be assumed.

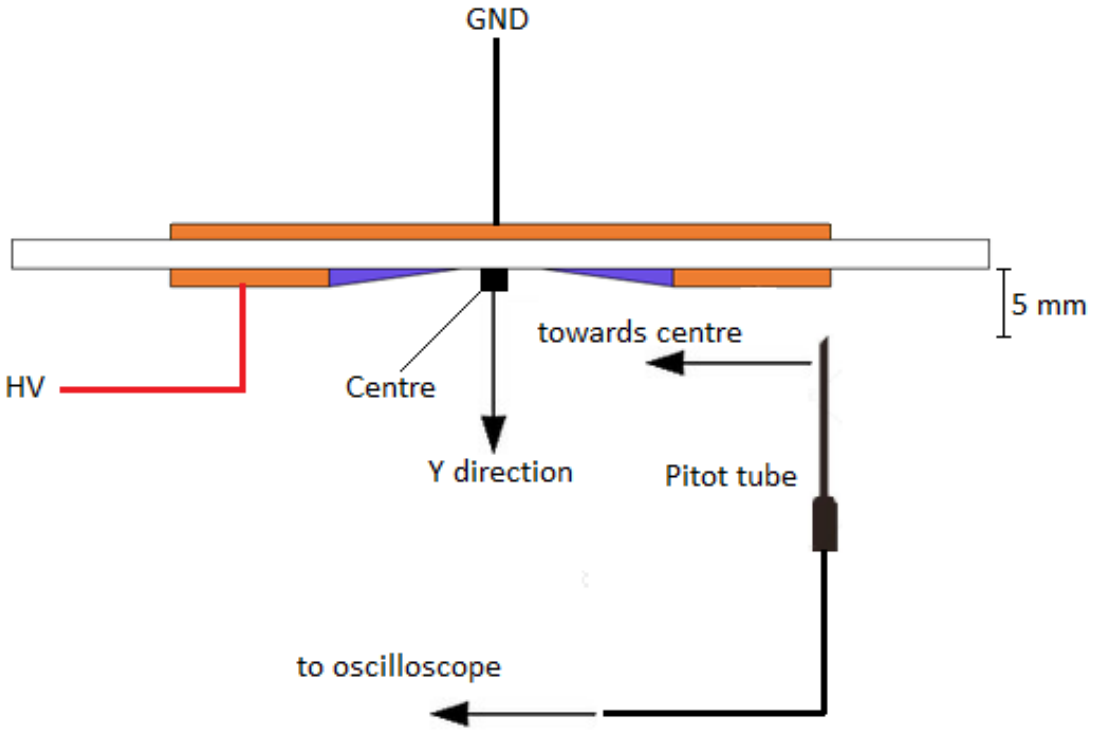

Figure 23. Experimental setup for velocity measurements.

Synthetic jets velocity profiles for devices with different electrode diameter were measured using a home-built glass Pitot tube placed at 5mm from plasma and moved by a step motor in direction parallel to dielectric (figure 23). Pitot tube was connected to a DCAL401 Sursense pressure transducer and voltage trace was recorded on a RIGOL DS4024 digital oscilloscope connected to a personal computer. All measurements were filtered by means of a first order RC low-pass filter with 100Hz cut-off frequency. Experiments were performed five times and standard deviations between measurements was found to be <10%.

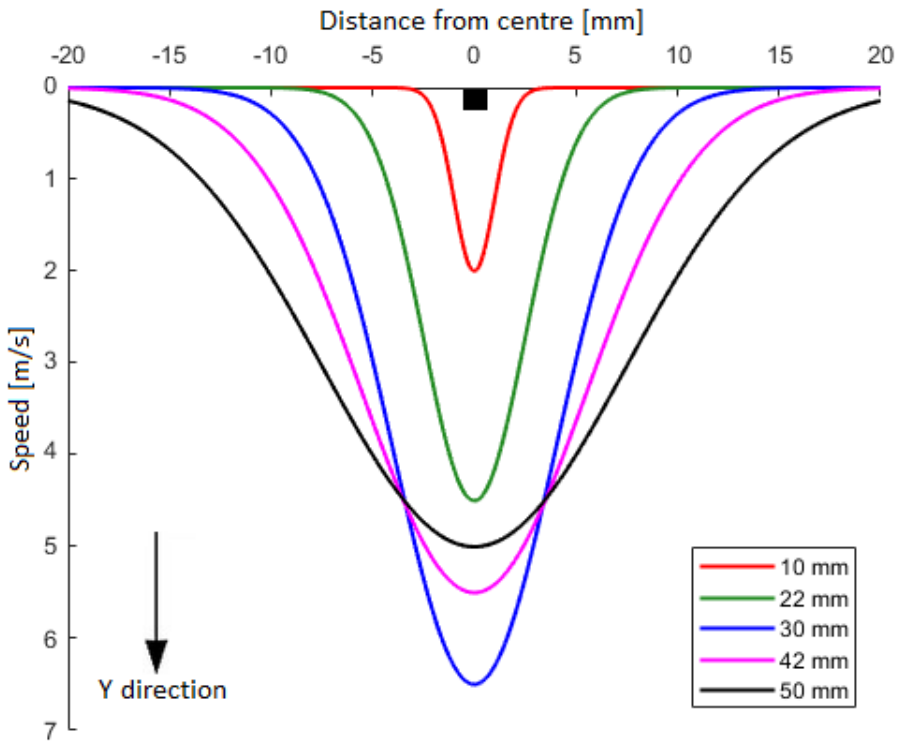

Figure 24. Velocity field in Y direction for devices with different electrode diameter operated in continuous mode.

Pitot tube diagnostic revealed that smaller devices impart less momentum to background atmospheric-pressure air, resulting in narrower and slower synthetic jets (figure 24). As electrode diameter increases, synthetic jets width and speed increase as well. However, increasing electrode diameter beyond critical value of 30mm results in decreased velocity (figure 25).

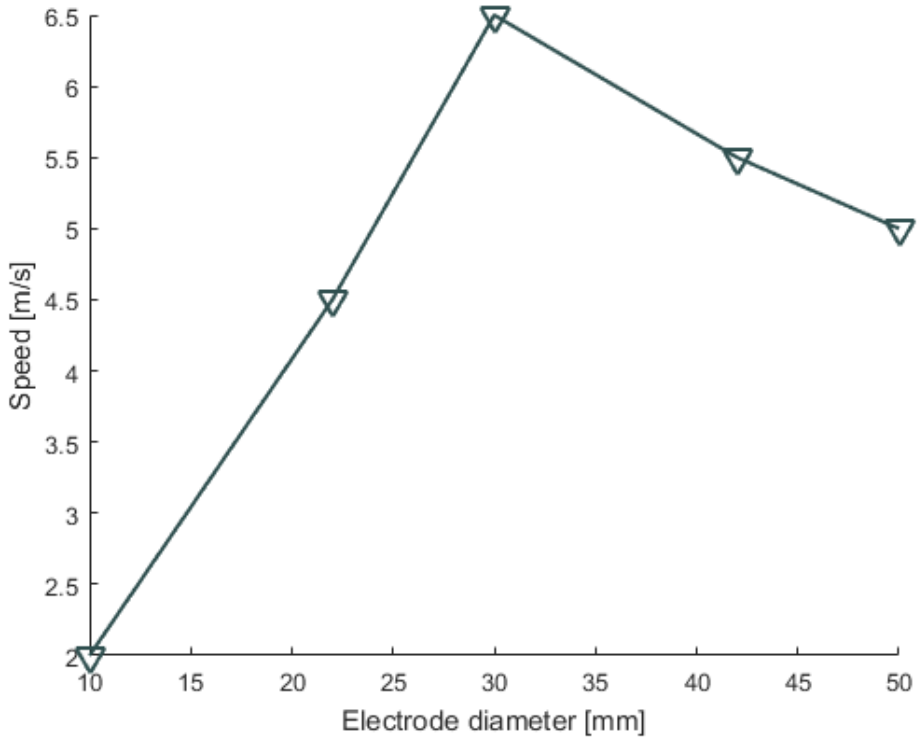

Figure 25. Synthetic jets maximum velocity as a function of electrode diameter for devices operated in continuous mode.

Schlieren imaging was used to visualise synthetic jets produced by annular surface dielectric barrier discharge devices. Schlieren photography is able to detect refractive index variations in fluids caused by density gradients. Schlieren pictures can therefore visualise warm mass fluxes produced in annular surface dielectric barrier discharges due to electrohydrodynamic body forces.

In Schlieren imaging setups, a collimated light beam is focused on target object with converging optical elements like parabolic mirrors and a knife-edge is placed in focal point. In uniform density fluids, this leads to a simple bright picture, though. In fluids with density gradients, light beam is distorted and therefore light that is focused in area covered by knife-edge is blocked. The result is a set of lighter and darker patches corresponding to positive and negative fluid density gradients in direction perpendicular to knife-edge.

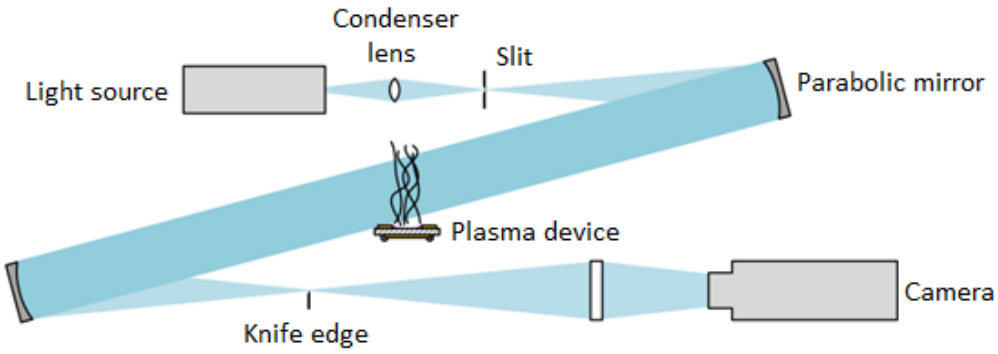

Figure 26. Experimental setup for Schlieren imaging.

Schlieren pictures of annular surface dielectric barrier devices were taken using a so-called Z-type setup (figure 26). Camera was connected to a personal computer and triggered with increasing delays after plasma ignition by means of a RIGOL DS4024 digital oscilloscope to obtain a set of pictures displaying complete synthetic jets development. Camera exposure time was set at 1ms and background reference pictures without plasma were taken as well.

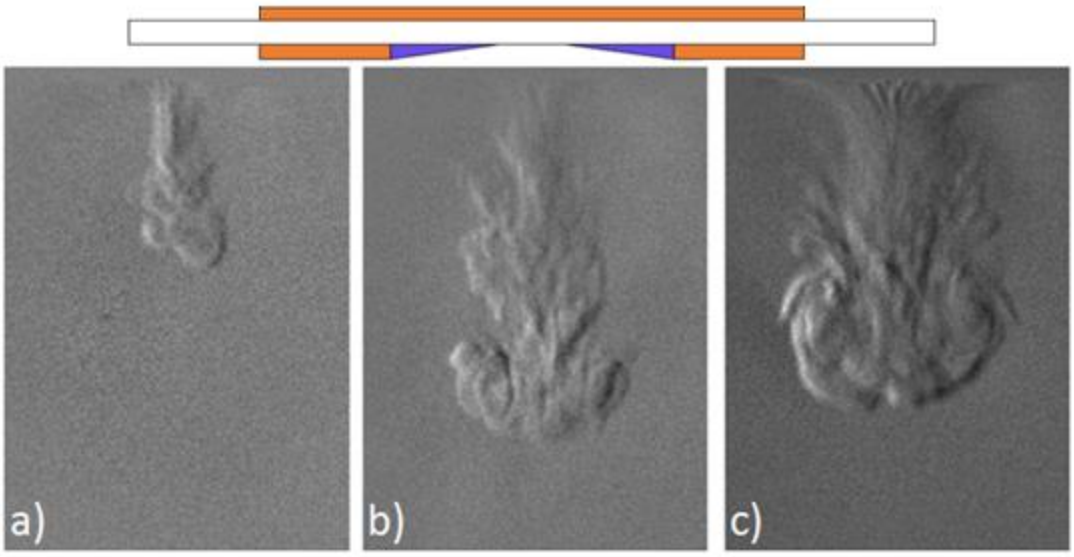

Figure 27. Schlieren pictures taken 40ms after plasma ignition in devices with a) *d* = 10mm, b) *d* = 30mm and c) *d* = 50mm operated in continuous mode.

Schlieren imaging confirmed results from Pitot tube measurements already discussed (figure 27). Annular surface dielectric barrier discharge device with 30mm

electrode diameter outperforms other arrangements, producing a faster synthetic jet and therefore being able to enhance electrohydrodynamic interaction.

To conclude, Schlieren pictures suggest that decreasing performance for devices with electrode diameter larger than 30mm might be caused by increased turbulence. Conversely, in smaller electrode diameter devices, discharge has not enough time to fully develop and therefore to efficiently impart momentum to background atmospheric-pressure air, as two positively charged surface plasmas coming opposite sides tend to repel each other.

Chapter 4
Reactive species delivery in annular surface dielectric barrier discharges

Reactive species delivery provided by fabricated annular surface dielectric barrier discharge devices was investigated performing aqueous indigo dye solutions degradation experiments. Changes in indigo degradation rate are related to variations in plasma reactive species mass transport to liquid. All the results that follows were obtained powering devices with a 11.5kV$_p$ sinusoidal voltage at 5kHz both in continuous and discontinuous mode to ensure constant plasma local properties throughout all experiments, as already discussed in Chapter 1.

Indigo is a well-known blue vat dye used in denim industry. Its water-soluble derivatives, such as indigo trisulfonate, are commercially available reagents listed as pH or redox indicators. Indigo trisulfonate aqueous solutions absorb light at about 605nm with a rather high molar absorbance. Indigo molecule contains only one carbon-carbon double bond that react with ozone produced in cold atmospheric-pressure air plasmas with high reaction rate.

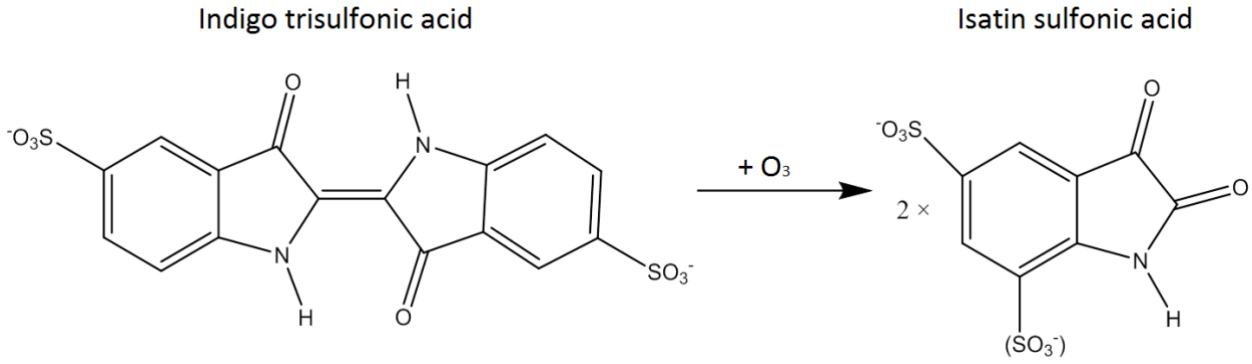

Figure 28. Aqueous indigo trisulfonate and its ozonation product.

At low pH values, amino groups are protonated and are therefore unreactive with ozone. Thus, it can be assumed that one molecule of indigo trisulfonate reacts with one molecule of ozone under proper reaction conditions, including reagents good mixing. Ozonation of indigo trisulfonate produces sulfonic compounds (figure 28) that are no longer able to absorb light at 605nm due to their very low molar absorbance at this wavelength. Light intensity at 605nm can therefore be related to indigo trisulfonate concentration in liquid and used to determine indigo degradation rate.

Potassium indigo trisulfonate (Sigma-Aldrich) test solutions (150ml, 5μM) were poured into a 45mm high PVC cylindrical container with inner diameter of 52mm (figure 29). Collimating lenses were mounted facing each other on containment walls to transmit and receive light emitted by an Ocean Optics HL-2000-FHSA tungsten-halogen lamp.

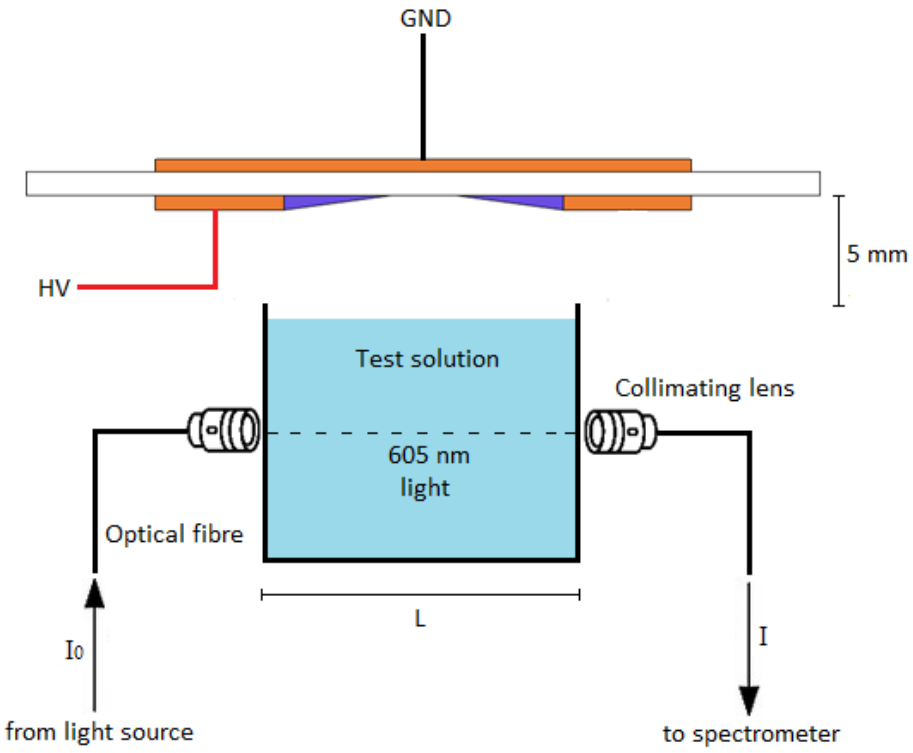

Figure 29. Experimental setup for indigo degradation experiments.

The container was placed coaxially underneath annular surface dielectric barrier devices at a fixed distance of 5mm from plasma. Time-resolved light intensity at 605nm was measured by means of a UV/VIS optical fibre connected to an Ocean Optics USB2000+ spectrometer. Detected light was assumed to follow Beer-Lambert law, thereby allowing to evaluate time-resolved indigo concentration as

$$C_{indigo} = \frac{\ln\left(\frac{I_0}{I}\right)}{\varepsilon L}$$

where I_0 is light intensity at 605nm provided by lamp, I is light intensity at 605nm after interaction with indigo test solution, ε = 23800 M/cm is indigo trisulfonate molar absorbance at 605nm [41] and L = 5.2cm is light optical path length within liquid.

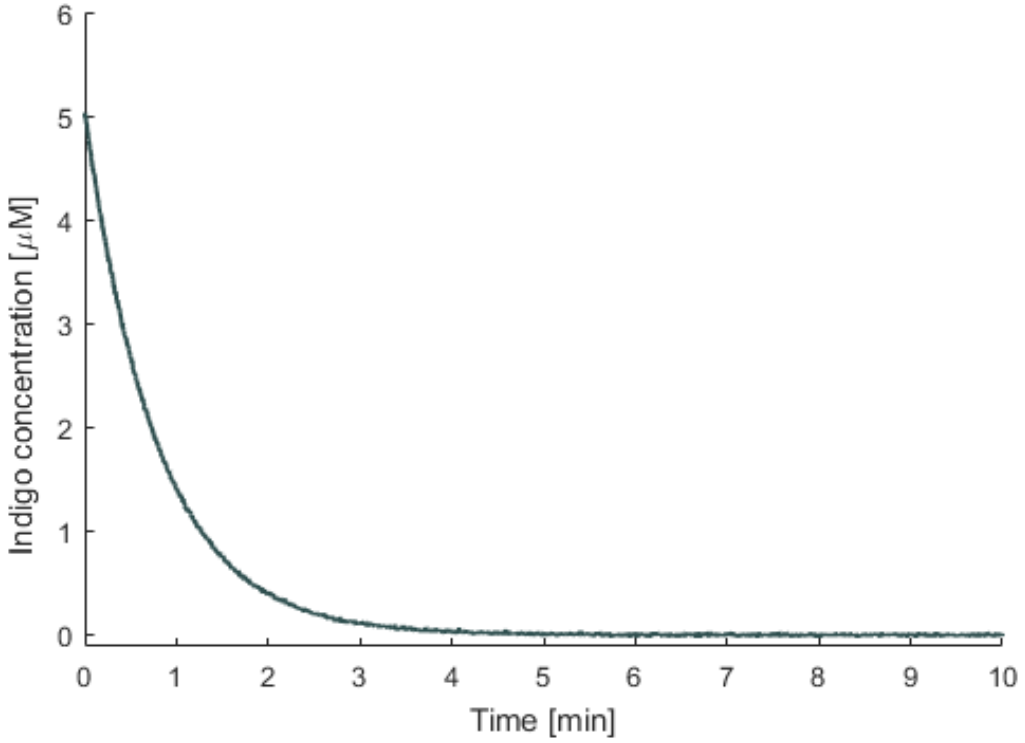

Figure 30. Time-resolved degradation curve of a 5μM potassium indigo trisulfonate solution provided by the 30mm electrode diameter device operated at 50% duty cycle.

All the degradation experiments were performed in an enclosure that prevented external crossflows and ensured reduced background light interference. A magnetic stirrer was used to guarantee good mixing of plasma reactive species into

liquid as well. Indigo degradation rate was determined as slope of indigo trisulfonate time-resolved concentration in liquid (figure 30). Experiments were performed in triplicate and standard deviation between measurements was found to be <6%.

Based on data presented in Chapter 1 and neglecting electrohydrodynamic effects, it would expected that, for fixed repetition frequency and duty cycle, indigo solutions degradation rate would linearly increase with electrode diameter. This linear increase would be attributed to longer plasmas forming in larger electrode devices. However, indigo solutions degradation rate dependence on electrode diameter is not linear and a nearly three-fold enhanced performance was observed for 30mm electrode diameter device (figure 31). Higher duty cycle operation of devices results in faster indigo degradation because of increased average power absorbed by plasma, which lead to higher reactive species production [42].

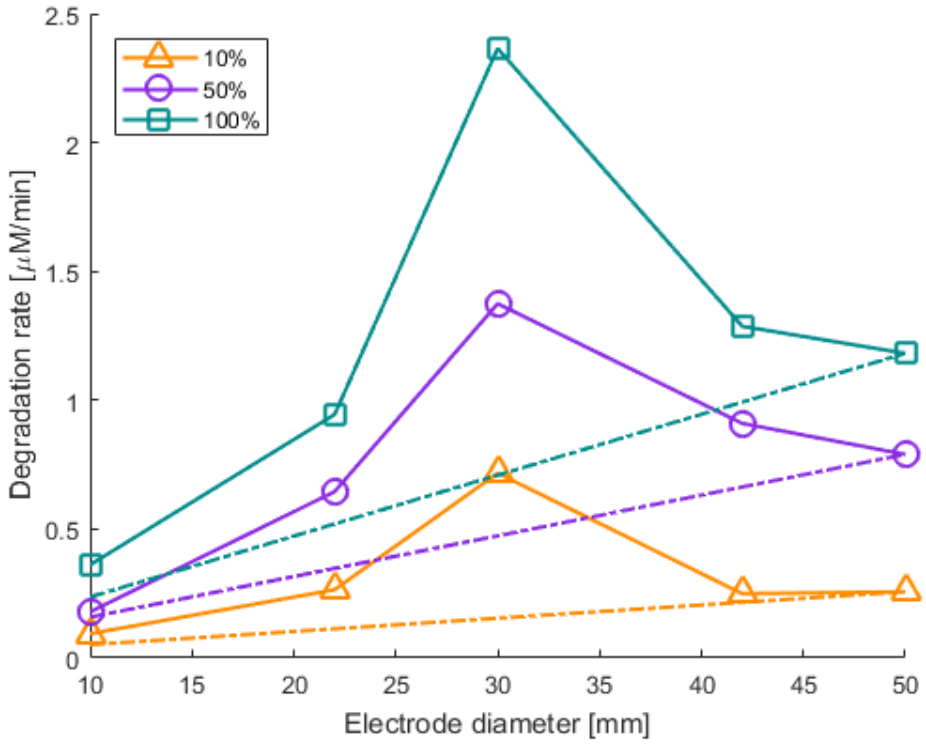

Figure 31. Degradation rate of 5µM potassium indigo trisulfonate solutions as a function of electrode diameter provided by devices operated at different duty cycle.

Enhanced performance provided by 30mm electrode diameter device implies that an increased plasma reactive species flux reaches indigo solution. Since plasma reactive species flux φ can be expressed as

$$\varphi = Cv$$

where C is reactive species concentration and v is their velocity component perpendicular to liquid surface, an increase in flux might be caused by both an increase in reactive species concentration or in synthetic jet speed.

To gain further insights into underlying mechanisms leading to enhanced mass transport in 30mm electrode diameter device, ozone production in annular surface dielectric barrier discharge devices operated in different conditions was investigated as well. Ozone was chosen because it can be measured non-intrusively by UV absorption method and, most importantly, it plays the major role in indigo degradation chemistry [43].

UV light absorption is the most widely accepted method for monitoring ozone concentration. It is highly-selective and can be applied to determine ozone both in gas and liquid phase. Ozone presents a strong UV absorption cross-section that peaks at almost 254nm in Hartley band (figure 32). Light intensity at 254nm can therefore be used to determine ozone concentration.

The measurements were performed by means of two UV/VIS optical fibres separated by 72mm (figure 33). The fibres faced each other 30mm away from plasma device and were terminated with collimating lenses. An Ocean Optics LLS-255 lamp was used as UV radiation source and light intensity was recorded by an Ocean Optics HR2000+ spectrometer.

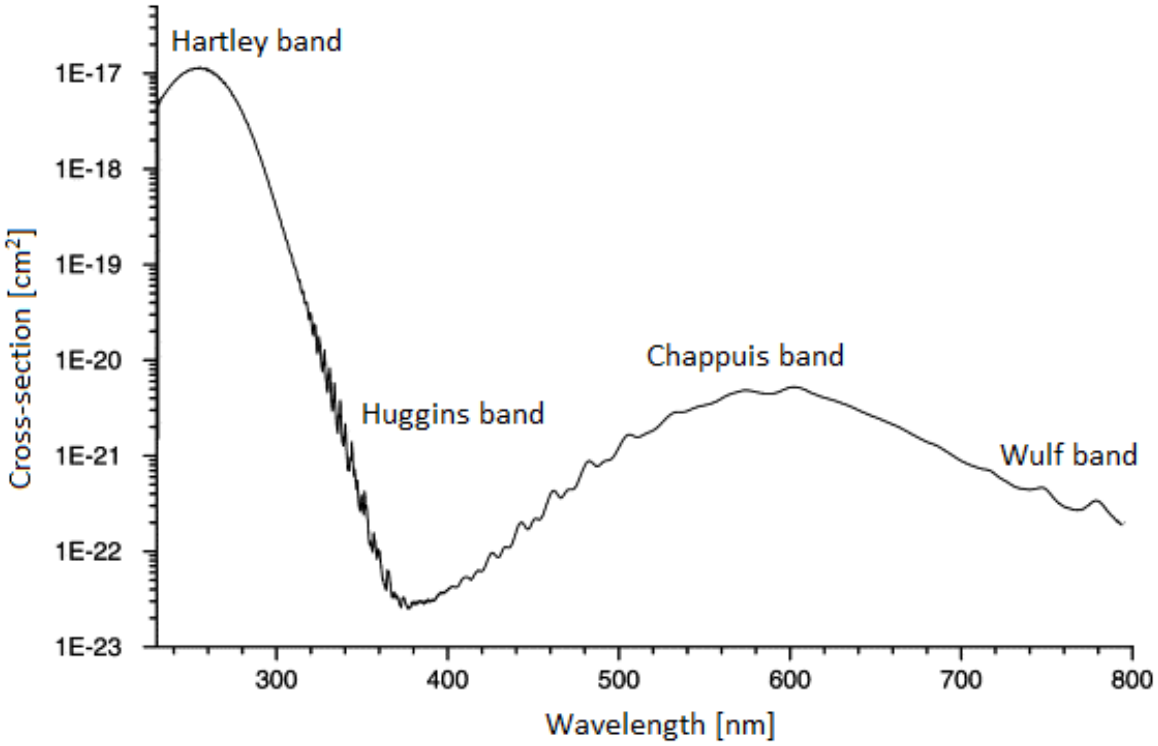

Figure 32. Ozone absorption cross-section.

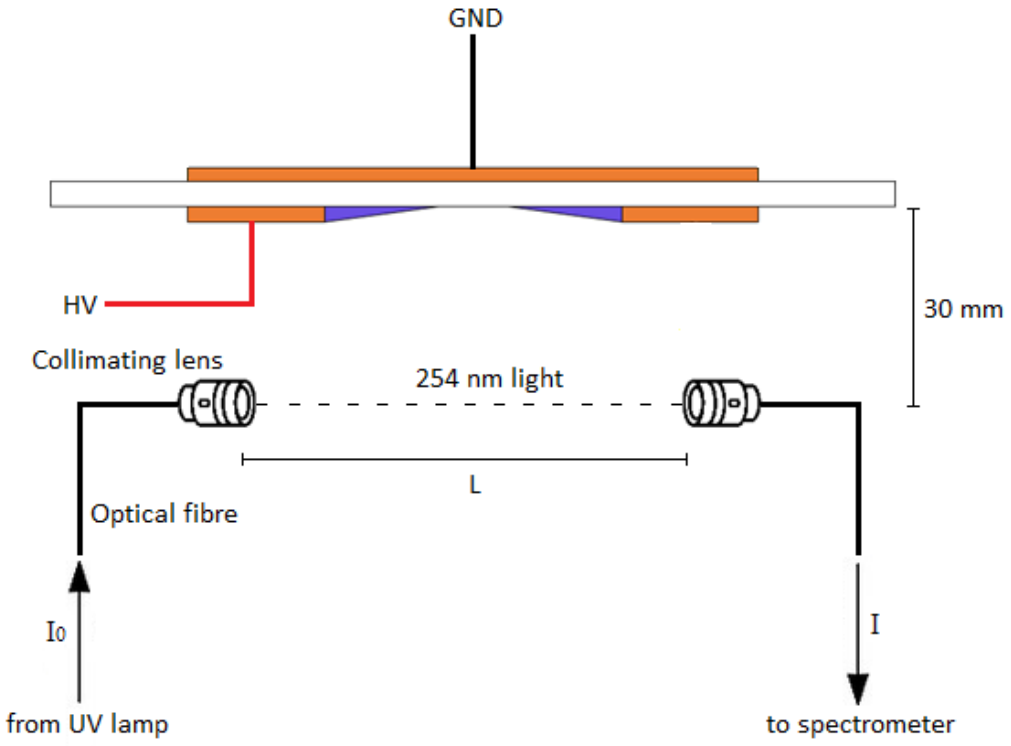

Figure 33. Experimental setup for ozone concentration measurements.

Detected light was assumed to follow Beer-Lambert law, thereby allowing to evaluate time-resolved ozone concentration (figure 34) as

$$C_{O_3} = \frac{\ln\left(\frac{I_0}{I}\right)}{\sigma L N}$$

where I_0 is light intensity at 254nm provided by lamp, I is light intensity at 254nm after interaction with O_3 molecules, σ = $1.12 \cdot 10^{-17} cm^2$ is ozone absorption cross-section at 254nm [44], L = 5.2cm is light optical path length and N = $2.504 \cdot 10^{19} cm^{-3}$ is atmospheric-pressure background air particle number density. Experiments were performed five times and standard deviation between measurements was found to be <10%.

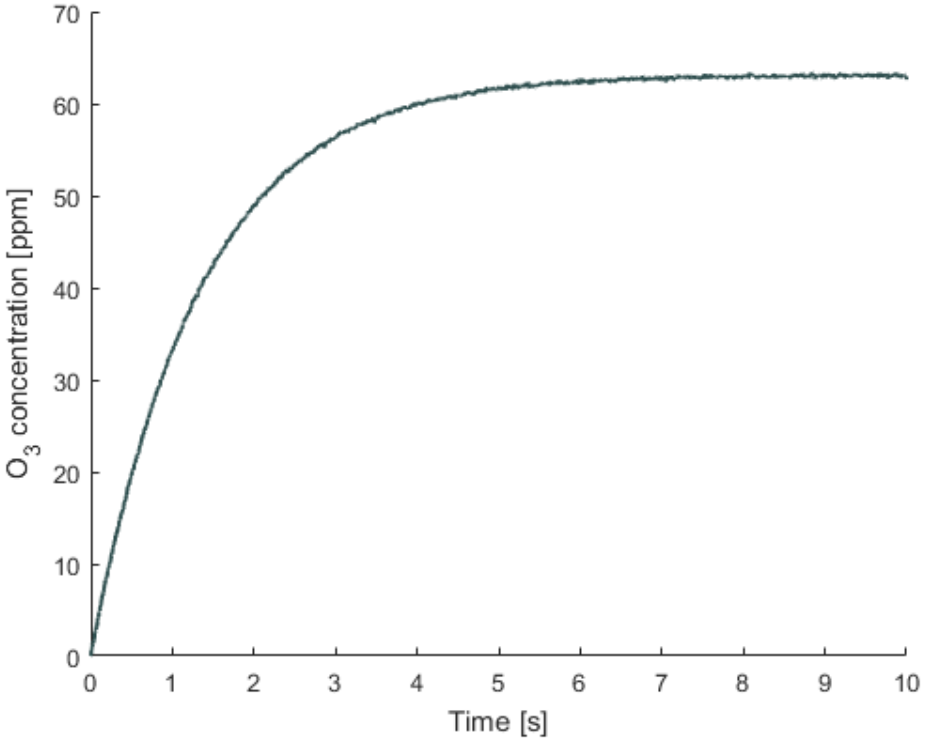

Figure 34. Time-resolved ozone concentration measured 30mm away from plasma generated by the 30mm electrode device operated at 50% duty cycle.

Since, as demonstrated in Chapter 1, devices driven at same modulation frequency and duty cycle operate at constant linear power density and temperature, discharge chemistry per unit length is expected to be the same. In other words, in

absence of non-local effects in afterglow, ozone concentration is supposed to increase linearly with electrode diameter for devices driven under same excitation conditions.

Indeed measured average ozone concentration was found to increase linearly with electrode diameter (figure 35) for discharges operated at same modulation frequency and duty cycle. Most importantly, no deviation from this linear behaviour was observed in 30mm electrode diameter device.

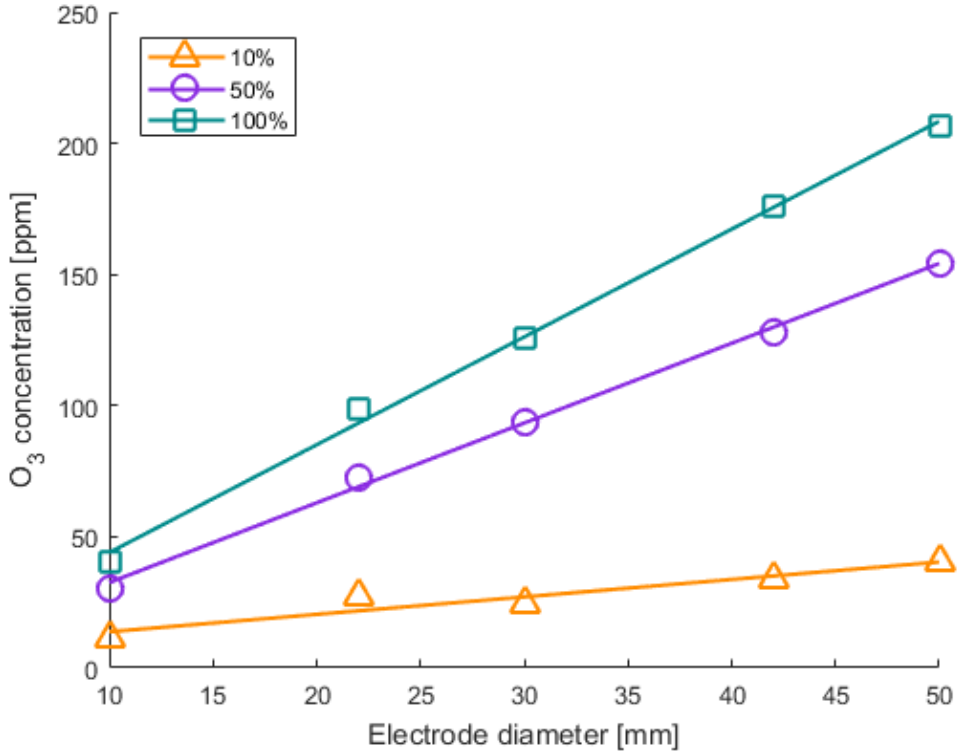

Figure 35. Ozone concentration measured 30mm away from plasma as a function of electrode diameter produced by devices operated at different duty cycle.

It must be noted that input power used in experiments was low enough to avoid a mode transition [45]. Since, as seen in Chapter 1, duty cycle has a direct influence on average power delivered to discharge and ozone generation in atmospheric-pressure air plasmas is strictly related to input power, measured ozone concentration consequently depends on duty cycle as well.

To conclude, ozone concentration measurements demonstrated that indigo solutions enhanced degradation caused by 30mm electrode diameter device is due to an increased reactive species delivery velocity rather than to an increase in their concentration. This enhanced velocity is provided by formation of a faster synthetic jet in 30mm electrode diameter device, as already demonstrated in Chapter 2.

Chapter 5
Inactivation of *Candida albicans* by annular surface dielectric barrier discharges

Candida albicans is one of the main fungal species with ability to grow as a biofilm on almost all surfaces, such as medical devices and human epithelial layers [46,47]. In the last decade, *Candida albicans* has shown increased levels of resistance to a wide spectrum of conventional antifungal drugs used in clinical practice [48].

Several studies demonstrated that environmental contamination by microbes that originate in dust and soil is a major problem where maintenance of a high level of hygiene is necessary, such as in hospitals or food-processing facilities [49].

Conventional sterilisation methods have been demonstrated to be less effective against biofilms [50,51]. Therefore, research efforts must be addressed to development of new antimicrobial strategies, especially for killing of microorganisms growing in biofilms.

A novel approach in inactivating pathogenic microorganisms is represented by cold atmospheric-pressure plasmas, which have demonstrated strong bactericidal, virucidal and fungicidal properties [52,53]. Plasma efficacy is dependent on exposure time, cell type and density, device used and its operating parameters.

Only recently inactivation of *Candida* biofilms using different cold atmospheric-pressure plasma devices has been carried out [54]. In this work *Candida albicans* was exposed to synthetic jet produced in an annular surface dielectric barrier discharge devices studied in previous chapters in order to evaluate their biocidal efficacy.

As shown in Chapter 4, 30mm electrode diameter annular surface dielectric barrier discharge device is the one enhancing reactive species mass transport to target under treatment. Therefore, it was chosen as preferred embodiment for this biological investigation.

Candida albicans cells were homogeneously spread onto agar culture inside a 90mm diameter polystyrene Petri dish and placed coaxially underneath plasma device at 15mm distance from dielectric layer (figure 36).

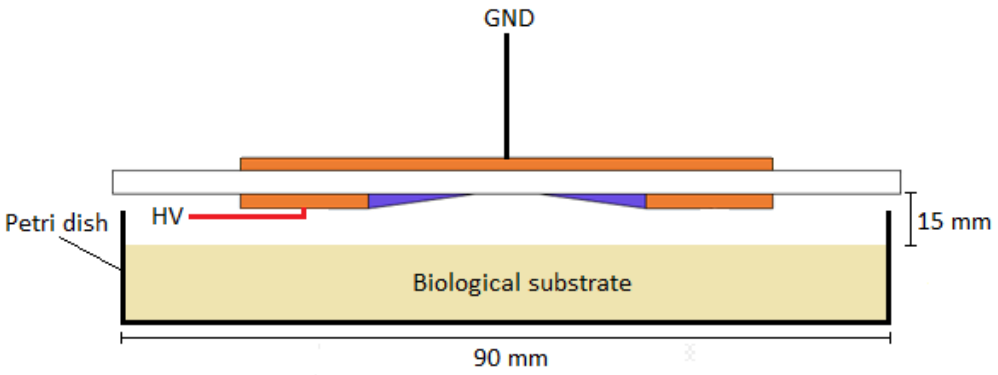

Figure 36. Experimental setup for *Candida albicans* inactivation tests.

For the sake of coherence, discharge was ignited in atmospheric-pressure quiescent air in the same operating conditions used to carry out all other experiments shown in this study.

As described in pervious chapters, plasma was excited in discontinuous mode by a 11.5kV$_p$ sinusoidal voltage at 5kHz. Modulation frequency and duty cycle were set at 500mHz and 50%, respectively. As seen in Chapter 2, average power absorbed by plasma is ~4W in these operating conditions.

Candida albicans was treated for 30s, 2min and 5min, respectively. One control sample was prepared for each condition. Cells concentration before and after plasma exposure were counted using a microscope. Treatments were performed in triplicate and standard deviation between measurements was estimated to be <2%.

Plasma exposure of *Candida albicans* to 30mm electrode diameter device resulted in a decreased cell concentration over treatment time (figure 37). A 5-log reduction in the bacterial load was recorded after 5min of plasma treatment.

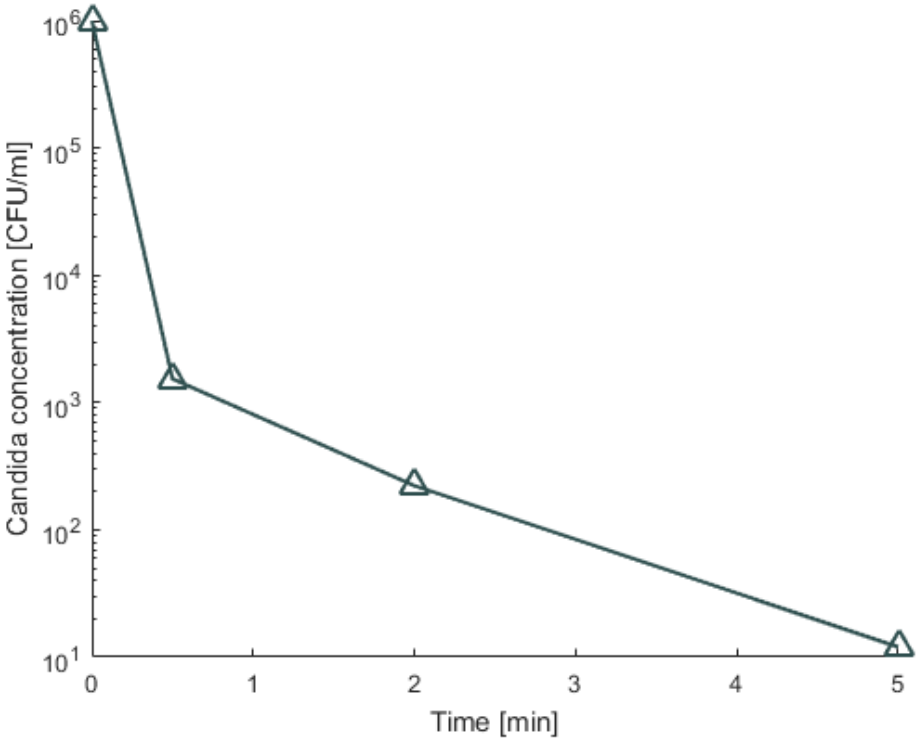

Figure 37. Survival curve of *Candida albicans* exposed to plasma generated in the 30mm electrode diameter device operated at 50% duty cycle.

In plasma-assisted sterilisation, clear understanding of inactivation mechanism to improve and optimize the process is crucial. A possible explanation of *Candida albicans* inactivation provided by annular surface dielectric barrier discharge plasma is given in what follows.

Charged particles and electric fields does not contribute to inactivation process in this case, since plasma is not in direct contact with biological substrate under treatment. Thermal effects can be considered negligible as well, because reactive species flux directed towards sample is characterised by temperatures much lower than those needed to obtain thermal sterilisation.

UV radiation emitted by plasma discharge cannot contribute either, since atmospheric-pressure air presents high UV absorbance and optical path between device and target is quite long. Therefore, it is very likely that major fraction of UV photons coming from plasma are absorbed by air molecules along their path towards biological sample. Nonetheless, as seen in Chapter 4, synthetic jet produced by annular surface dielectric barrier discharges contains a large amount of ozone molecules that highly absorb UV light as well, especially in the 240-260nm band, which turns out to be the useful one for biocidal purposes.

In conclusion, *Candida albicans* inactivation process assisted by annular surface dielectric barrier discharges is therefore dominated by oxidising action upon cell membranes provided by reactive oxygen and nitrogen species delivered to sample by synthetic jets. As seen in Chapter 1, chemical compounds produced in atmospheric-pressure air electric gas discharges are powerful tools in damaging cell membranes and, consequently, in causing pathogens death.

Chapter 6
Conclusions

Cold atmospheric-pressure plasmas are chemically reactive media that show promising antimicrobial effects. Although detailed biochemical mechanisms leading to microorganisms inactivation are still unclear, a wide variety of biological applications of low-temperature plasmas have been developed over the last two decades.

In particular, surface dielectric barrier discharge plasmas have recently attracted renewed interest for emerging applications in biomedical, environmental and food sectors. Reactive species delivery to samples being treated is pivotal in these applications. Mass transport in surface dielectric barrier discharges is typically assumed to be diffusion-controlled. However, this work demonstrates that electrodes can be engineered to take advantage of electrohydrodynamic forces and enhance the process.

Novel annular surface dielectric barrier discharge devices with different electrode diameter were fabricated and operated in atmospheric-pressure air, leading to formation of a reactive oxygen and nitrogen species flux perpendicular to insulating surface. Devices were powered in different operating conditions and investigated by means of several experimental techniques, including electrical measurements, optical emission spectroscopy, Pitot tube diagnostic and chemical essays.

For annular surface dielectric barrier discharges studied in this work, a 3-fold improved efficacy from what would otherwise be supposed from power and plasma size considerations was observed for 30mm electrode diameter device. Similar effects

are expected in devices with different electrode patterns and further research efforts should therefore address not only optimisation of a single synthetic jet, but also interaction between multiple jets in view of a scale-up.

Biocidal efficacy of annular surface dielectric barrier discharges was tested as well by exposing *Candida albicans* to 30mm electrode diameter device. A 5-log reduction in the bacterial load was obtained after only 5min of treatment powering plasma with less than 4W.

As low power consumption, simple scalability and versatility of application are distinctive features of annular surface dielectric barrier discharges, this result could pave the way for development of plasma devices able to perform in-field large area treatments.

References

[1] Matthews I P, Gibson C and Samuel A H, 1994 *Clin. Mater.* **15**

[2] Ehlbeck J et al, 2011 *J. Phys. D: Appl. Phys.* **44**

[3] Lerouge S, Tabrizian M, Wertheimer M R, Marchand R and Yahia L, 2002 *Biomed. Mater. Eng.* **12**

[4] Ermolaeva S A et al, 2011 *J. Med. Microbiol.* **60**

[5] Li Y F, Shimizu T, Zimmermann J L and Morfill G E, 2011 *Plasma Process. Polym.* **11**

[6] Shimizu T, Zimmermann J L and Morfill G E. 2011 *New J. Phys.* **13**

[7] Maisch T et al, 2012 *PLoS One* **7**

[8] Heinlin J et al, 2011 *J. Eur. Acad. Dermatol. Venereol.* **25**

[9] Isbary G, Morfill G E, Zimmermann J, Shimizu T and Stolz W, 2011 *Arch. Dermatol.* **147**

[10] Isbary G et al, 2010 *Br. J. Dermatol.* **163**

[11] Gaunt L F, Beggs C B and Georghiou G E, 2006 *IEEE Trans. Plasma Sci.* **34**

[12] Laroussi M and Leipold F, 2004 *Int. J. Mass Spec.* **233**

[13] Weltmann K D and von Woedtke T, 2017 *Plasma Phys. Control. Fusion* **59**

[14] Graves D B, 2012 *J. Phys. D: Appl. Phys.* **45**

[15] Shintani H, Sakudo A, Burke P and McDonnel G, 2010 *Exp. Ther. Med.* **1**

[16] Kong M G, Kroesen G, Morfill G E, Nosenko T, Shimizu T, van Dijk J and Zimmerman J L, 2009 *New J. Phys.* **11**

[17] Ikawa S, Tani A, Nakashima Y and Kitano K, 2016 *J. Phys. D: Appl. Phys.* **49**

[18] Foster J E, Sommers B S, Gucker S N, Blankson I M and Adamovsky G, 2012 *IEEE Trans. Plasma Sci.* **40**

[19] Siemens W, 1857 *Poggendorff 's Ann. Phys. Chem.* **102**

[20] Neretti G, Taglioli M, Colonna G and Borghi C A, 2017 *Plasma Sources Sci. Technol.* **26**

[21] Kogelschatz U, 2003 *Plasma Chem. Plasma Process.* **23**

[22] Moreau E, 2007 *J. Phys. D: Appl. Phys.* **40**

[23] Santhanakrishnan A and Jacob J D, 2007 *J. Phys. D: Appl. Phys.* **40**

[24] Neretti G, Cristofolini A and Borghi C A, 2014 *J. Appl. Phys.* **115**

[25] Morfill G E, Shimizu T, Steffes B and Schmidt H U, 2009 *New J. Phys.* **11**

[26] Williamson J M, Trump D D, Bletzinger P and Ganguly B N, 2006 *J. Phys. D: Appl. Phys.* **39**

[27] Mitra A, Li Y F, Klämpfl T G, Shimizu T, Jeon J, Morfill G E and Zimmermann J L, 2014 *Food Bioprocess Technol.* **7**

[28] Shaw A, Shama G and Iza F, 2015 *Biointerphases* **10**

[29] Liu D X, Liu Z C, Chen C, Yang A J, Li D, Rong M Z, Chen H L and Kong M G, 2016 *Sci. Rep.* **6**

[30] Sakiyama Y, Graves D B, Chang H-W, Shimizu T and Morfill G E, 2012 *J. Phys. D: Appl. Phys.* **45**

[31] Shaw A, Seri P, Borghi C A, Shama G and Iza F, 2015 *J. Phys. D: Appl. Phys.* **48**

[32] Potts H E, Diver D A, Everest P C and O'Connor R D, 2011 *Proc. of 30th Int. Conf. on Phenomena in Ionized Gases*

[33] Dong L, Fan W, He Y, Liu F, Li S, Gao R and Wang L, 2006 *Phys. Rev. E* **73**

[34] Neretti G, Seri P, Taglioli M, Shaw A, Iza F and Borghi C A, 2017 *J. Phys. D: Appl. Phys.* **50**

[35] Taglioli M, Shaw A, Wright A, FitzPatrick B, Neretti G, Seri P, Borghi C A and Iza F, *Plasma Sources Sci. Technol.* **25**

[36] Enloe C L, McLaughlin T, Van Dyken R, Kachner K, Jumper E and Corke T C, 2004 *AIAA J.* **42**

[37] Manley T C, 1943 *J. Electrochem. Soc.* **84**

[38] Bruggeman P J, Sadeghi N, Schram D C and Linss V, 2014 *Plasma Sources Sci. Technol.* **23**

[39] Iza F and Hopwood J A, 2004 *IEEE Trans. Plasma Sci.* **32**

[40] Laux C O, 2008 *Optical Diagnostics and Collisional-Radiative Models*, Von Karman Institute Course on Hypersonic and Cruise Vehicles, Stanford University

[41] Bader H and Hoigné J, 1981 *Water Res.* **15**

[42] Kogelschatz U, Eliasson B and Egli W, 1997 *J. Phys. IV France* **7**

[43] Bruggeman P J et al, 2016 *Plasma Sources Sci. Technol.* **25**

[44] Grebenshchikov S Y, Qu Z W, Zhu H and Schinke R, 2007 *Phys. Chem. Chem. Phys.* **9**

[45] Shimizu T, Sakiyama Y, Graves D B, Zimmermann J L and Morfill G E, 2012 *New J. Phys.* **14**

[46] Uppuluri P, Chaturvedi A K, Lopez-Ribot J L, 2009 *Future Microbiol.* **4**

[47] Vazquez J A et al, 1998 *J. Clin. Microbiol.* **36**

[48] Jori G et al, 2006 *Am. J. Infect. Control* **38**

[49] Donlan R M and Costerton J W, 2002 *Clin. Microbiol. Rev.* **15**

[50] Fux C A, Costerton J W, Stewart P S and Stoodley P, 2005 *Trends Microbiol.* **13**

[51] Hoyle B D and Costerton J W, 1991 *Prog. Drug Res.* **37**

[52] Shimizu T, Zimmermann J L and Morfill G E, 2011 *New J. Phys.* **13**

[53] Zimmermann J L et al, 2011 *J. Phys. D: Appl. Phys.* **44**

[54] Koban I et al, 2010 *New J. Phys.* **12**